Geochimica et Cosmochimica Acta 392 (2025) 175–194

Contents lists available at ScienceDirect

Geochimica et Cosmochimica Acta

journal homepage: www.elsevier.com/locate/gca

The role of scapolite-bearing granulites in sequestering and releasing sulfur: Implications for S isotope signatures of crustal fluids during lower-crustal exhumation

Johannes Hammerli [a,b,c,*], Anthony I.S. Kemp [d], Anne-Sophie Bouvier [e], Roberta L. Rudnick [f], Pierre Boivin [g], Robert M. Holder [h], Thomas Chacko [i], Kevin Blake [j]

[a] School of the Environment, Washington State University, Pullman, WA, USA
[b] University of Bern, Institute of Geological Sciences, Bern, Switzerland
[c] Geoscience, James Cook University, Townsville, QLD, Australia
[d] School of Earth Sciences, University of Western Australia, Perth, Australia
[e] Institute of Earth Sciences, University of Lausanne, Lausanne, Switzerland
[f] Department of Earth Science and Earth Research Institute, University of California, Santa Barbara, CA, USA
[g] Université Clermont Auvergne, CNRS, IRD, OPGC, Laboratoire Magmas et Volcans, Clermont-Ferrand, France
[h] Department of Earth and Environmental Sciences, University of Michigan, Ann Arbor, MI, USA
[i] Department of Earth and Atmospheric Sciences, University of Alberta, Edmonton, Canada
[j] Advanced Analytical Centre, James Cook University, Townsville, Qld 4811, Australia

ARTICLE INFO

Associate editor: Lifei Zhang

Keywords:
Scapolite-bearing granulite
Sulfur isotopes
Scapolite
S-rich apatite
S budget of the lower crust
Volatile transfer between mantle and crust

ABSTRACT

To understand sulfur and carbon sequestration and release within the continental crust, scapolite minerals from a variety of granulite facies rocks were analyzed for their elemental composition and S isotope signatures. These high-grade scapolites host significant amounts of SO_3 and CO_2, up to approximately 5 wt% and 3 wt%, respectively, with $\delta^{34}S_{VCDT}$ from −3 to +10 ‰, and formed in relatively oxidizing environments characterized by low aH_2O in which scapolite may form as a primary igneous mineral or via metamorphic reactions involving sulfides and silicates. The range of scapolite sulfur isotope compositions mirrors those observed in mantle xenoliths, suggesting transport of S from the mantle into the lower crust via fluids and melts. Although scapolite's contribution to the global S and C cycles may be modest, it is significant in the context of sulfur fluxing from the mantle to the lower crust, particularly in its oxidized form. We estimate that at least 10 % of lower crustal sulfur is sequestered within scapolite. The exhumation of scapolite-bearing lower crustal rocks can therefore liberate substantial quantities of sulfur species and CO_2, which may serve to both supply and compositionally buffer retrograde metamorphic fluids. These fluids may exhibit a range of S isotope compositions from mantle-like ($\delta^{34}S_{VCDT} \approx 0$ ‰) to relatively ^{34}S-enriched signatures. Consequently, retrograde fluids may have S isotope signatures indistinguishable from those of mantle fluids, even in the absence of direct mantle S input during fluid formation. Exhumation of scapolite-bearing lower crust may facilitate element mobilization through S and Cl complexing, particularly with respect to base metals, within exhumed lower crustal sections, thus providing sources of metals and fluids in mid- to high-grade metamorphic rocks. Globally, scapolite-bearing lower crust may help balance the global sulfur cycle through catch-and-release from scapolite.

1. Introduction

Scapolite-group minerals play a significant role in the volatile budget of lower crustal granulites. These minerals are the only major mineral phase in lower crustal rocks capable of hosting substantial quantities of sulfate and may also serve as an important reservoir for carbonate. They occur in a range of lithologies, from mafic granulites to calc-silicates (Newton and Goldsmith, 1975; Goldsmith, 1976). Indeed, Goldsmith (1976) states that "*It is not too far-fetched to assume that most of the CO_2 (and SO_2) in the air we breathe, and therefore the carbon in our bodies, has at one time been in scapolite.*" This supposition is based on the recognition that scapolite, a common rock-forming mineral in deep crustal rocks,

* Corresponding author.
E-mail address: johannes.haemmerli@wsu.edu (J. Hammerli).

https://doi.org/10.1016/j.gca.2025.01.010
Received 5 August 2024; Accepted 10 January 2025
Available online 13 January 2025

can contain several weight percent of sulfur and carbon, measured and reported as SO_3 and CO_2, respectively (von Knorring and Kennedy (1958), Lovering and White (1964), Dawson (1968), Goldsmith and Newton (1977), Blattner and Black (1980), Rollinson (1980), Moecher et al. (1992, 1994), Moecher (1993); Markwick and Downes (2000), Yoshino and Satish-Kumar (2001), Mansur et al. (2014), and Porter and Austrheim (2017). Given these observations, it is important to quantify the mass of S and C hosted by scapolite minerals, as well as their S isotopic signatures, to understand the global S and C cycles and, specifically, the exchange of these volatile elements between the mantle and lower crust to the surface. This is crucial as scapolite might be the most important mineral sequestering S, in its oxidized forms, in the deep crust (Qiu et al., 2021; Hamisi et al., 2023).

In metamorphic rocks, SO_4^{2-}-rich scapolite with a minor to major CO_3^{2-} component is only stable under lower crustal P-T conditions (Goldsmith and Newton, 1977; Almeida and Jenkins, 2017). During exhumation of high-grade rocks, or interaction of these rocks with retrogressive aqueous fluids, significant quantities of SO_4^{2-} and CO_2 can be released due to scapolite decomposition. This liberation of (oxidized) S and C generates mass transfer of both volatiles and metals within the middle crust. Sulfur is one of the most reactive elements in hydrothermal fluids, having a wide range of redox states from S^{2-} to S^{6+}. Given that most economically important metals in typical crustal rocks are concentrated within sulfides, the breakdown of sulfides in oxidizing environments can release these metals. Furthermore, as an important ligand for metals in solution, S plays a critical role in mobilizing metals and in the formation of hydrothermal base metal and precious metal deposits (e.g., Yardley, 2005; Mei et al., 2015; Rielli et al., 2018). Recently, Harlov (2024) emphasized the importance of sulfur in the lower crust and its role in granulite-facies metamorphism, oxidation, and the geochemical transformation of the deep crust. Scapolite breakdown in exhumed deep crustal rocks could supply S and C to retrograde fluids, which would then inherit the S and C isotope signature of scapolite. Interaction between such fluids and sulfides would generate a range of S isotope ratios. Since scapolite minerals can incorporate significant amounts of volatiles, they may sequester C and S when these volatiles interact with lower crustal rocks (Goldsmith, 1976). Scapolite in the lower crust may therefore account for a portion of the "missing" C and S of the global C and S budget (Bebout, 1996; Hilton et al., 2002, Wallace, 2005, Bekaert et al., 2021), which may be released during exhumation.

In this study, we analyzed the composition of scapolite minerals, including their S isotope signatures, via high spatial resolution micro-analytical techniques. We examined scapolite from granulites, of mafic to calc-silicate compositions and from volcanic-pipe xenoliths and scapolite phenocrysts in tephra. We also measured the isotopic composition of coexisting sulfides and apatite for comparison with scapolite. The results reveal that the lower crust has a heterogeneous sulfur isotope composition, ranging over 10 ‰ $\delta^{34}S$ vs. VCDT. We further conclude that scapolite can be an important reservoir of oxidized sulfur in the deep crust, hosting an estimated 10 % of the total sulfur of the lower continental crust.

2. Background

Scapolite group minerals are tectosilicates commonly present in rocks that interacted with high-salinity, and/or C and S-rich fluids. The formula of scapolite minerals is best described by $M_4(T_{12}O_{24})A$, where M represents Na, K, Ca, Sr, Ba and Fe^{2+}; T represents Si, Al and Fe^{3+}. The A-site is a so-called "cage-site", which is surrounded by rings of (Al,Si) tetrahedra providing space for halogens, SO_4^{2-} and CO_3^{2-} (Levien and Papike, 1976). Natural scapolite group minerals occur almost exclusively as solid solutions of several end-members. The sulfur scapolite end-member is silvialite ($Ca_4Al_6Si_6O_{24}SO_4$), whereas marialite is the sodium chloride end-member ($Na_4Al_3Si_9O_{24}Cl$) and the calcium carbonate end-member is meionite ($Ca_4Al_6Si_6O_{24}CO_3$) (Teertstra and Sherriff, 1997). Natural end-member scapolite group minerals have a relatively restricted stability field (e.g., Newton and Goldsmith, 1975, 1976; Almeida and Jenkins, 2017). Intermediate scapolite compositions, especially along the meionite and marialite solid solution, have a relatively large stability field and are common in a wide range of metamorphic settings, including high-grade metamorphic rocks, whereas SO_4^{2-}- and CO_3^{2-}-rich scapolite compositions have narrower stability fields restricted to lower crustal conditions (Newton and Goldsmith, 1976; Rakotondrazafy et al., 1996; Teertstra and Sherriff, 1997; Teertstra et al., 1999). Field evidence supports the experimental work, as SO_4^{2-}-rich scapolite has been exclusively found in granulite facies rocks and as xenocrysts in volcanic material (e.g., Lovering and White, 1964; Boivin and Camus, 1981; Torró et al., 2018). For SO_4^{2-}-rich scapolite, elevated aH_2O typically leads to its destabilization (e.g., Porter and Austrheim, 2017).

Given the intolerance of scapolite to high aH_2O, relatively anhydrous lower crustal lithologies are a favorable setting for the formation of scapolite group minerals when there is a sufficient supply of C and S. Although the composition of the lower crust continues to be debated (e.g., Hacker et al., 2015, Sammon et al. 2022), it exhibits a considerable degree of heterogeneity, encompassing a spectrum of rock types ranging from metasedimentary rocks to mafic granulites with cumulate-like characteristics (Rudnick and Fountain, 1995). Sulfur and C-rich scapolite minerals have been reported in almost all lower crustal rock-types and, as discussed below, different processes may form scapolite. Prior studies have indicated that sulfur in scapolite occurs predominantly in the S^{6+} state (e.g., Hamisi et al., 2023), offering insights into the redox conditions of the environments where scapolite forms. S-rich scapolite's relatively limited stability range, confined to the pressure and temperature conditions characteristic of the lower crust, makes it an intriguing mineral for investigating S (and C) isotopes and concentrations in this region. Notably, the preservation of S-rich scapolite implies minimal retrograde fluid-rock interaction, reducing the likelihood of disturbances in S isotope signatures. This is often challenging to avoid when working with whole-rock samples or sulfides, which are stable over a broader range of pressure–temperature conditions and where S exchange with fluids may be cryptic.

3. Methods

To ensure analytical accuracy, a combination of high spatial resolution micro-analytical techniques was applied in order to resolve zoning in minerals and to avoid altered zones and inclusions, such as sulfides (e.g., Korinevsky and Korinevsky, 2016). Analysis of unaltered zones of target minerals is particularly important for S isotope quantification, as sulfides may form during alteration of scapolite (Porter and Austrheim, 2017). The formation of such secondary minerals may generate significant S isotope fractionation that is not resolvable via bulk methods. Electron probe-microanalysis (EPMA) was used to determine major element composition and to map element distribution within individual grains, while secondary ionization mass spectrometry (SIMS) was used to measure S isotope ratios in scapolite, sulfides, and apatite. Most analyses were performed on petrographic thin sections in order to preserve the textural context, such as grain boundaries and scapolite inclusions in other rock-forming minerals.

3.1. Major element analysis via EPMA

Quantitative major element analyses of scapolite minerals were conducted by wavelength dispersive spectrometry using a JEOL JXA 8200 Superprobe housed at the Advanced Analytical Centre, James Cook University, Australia. Analyses employed a 15 kV acceleration voltage and 20nA beam current. A 5 μm diameter defocused beam was used to avoid potential diffusion of Na and Cl caused by the beam. Counting times were 20 s on peak and 10 s on background for each element. The data were processed using φρz corrections (Armstrong,

1991) and standardized against a set of well-characterized, in-house standards. Semi-quantitative EPMA maps of scapolite were produced with 20 kV acceleration voltage, a 20nA beam current and depending on the crystal size a step size of 2 to 5 μm. Most of the apatite grains were analyzed at the Centre for Microscopy, Characterisation and Analysis at the University of Western Australia following the method described in Parra-Avila et al. (2022). The apatite in mafic granulite xenolith sample 1636 (see below) was analyzed using a JEOL JXA-8900R EPMA at the University of Alberta, Canada. Details of the EPMA methodology and standards used for apatite analyses are listed are provided in the supplementary material.

3.2. Bulk grain S isotope analysis

We used the fluorination method for bulk grain sulfur isotope analyses. The sulfur isotope composition of two aliquots from the crystals CB2 and Alg-1 was determined by chemical extraction of total sulfur, followed by fluorination and dual-inlet gas-source isotope-ratio mass spectrometry. These analyses were performed at the Stable Isotope Laboratory in the Department of Earth and Planetary Sciences at McGill University, following the methodology described in Hammerli et al. (2017).

3.3. In situ SIMS measurements of S isotopes

3.3.1. Sample preparation

Scapolite, apatite and sulfide were extracted from 7 polished thin sections using an ultrasonic drill. The extracted ~3 mm diameter discs were pressed into Indium together with the scapolite reference materials CB1 (Hammerli et al., 2017), Alg-1 and CB2. Apatite and pyrite reference material were added to the mounts and these minerals were also measured for their S isotope compositions. A total of 10 sample mounts each containing one or more fragments of the reference material were prepared. All samples and reference materials were placed within ~8 mm of the center of the 1-inch diameter mount and polished flat to reduce primary and secondary beam deflections associated with the holder edge and topography (Kita et al., 2011).

3.3.2. SIMS Analyses

Sulfur isotopes in the scapolites were determined via Secondary Ion Mass Spectrometry (SIMS) using a Cameca 1280HR instrument at the SwissSIMS facility housed at the University of Lausanne over seven sessions (July 14–17 2020 and June 21–23 2021). A ~2nA Cs^+ primary ion beam was accelerated at 10 kV and focused on a 12 μm spot size. Secondary ions ^{32}S and ^{34}S were measured in multicollection mode, using two Faraday cups equipped with $10^{11}\Omega$ resistors. Each analysis consists of 60 cycles of detection for 4 s. Before each analysis, a 60 s pre-sputtering was applied, followed by automatic centering of the secondary ions beam.

To determine instrumental mass fractionation (IMF), reference material CB1 was used (Hammerli et al., 2017) and all scapolite analyses of unknowns were normalized to CB1 ($\delta^{34}S$ = 5.08 ‰ vs. VCDT). For the different sessions, the IMF was relatively similar, with values between 5.5 and 6 ‰. The final $\delta^{34}S$ was calculated for each measurement as follows: $\delta^{34}S_{final} = \delta^{34}S_{drift\ corrected} - IMF$. Magnetic field drift was monitored by bracketing the unknowns with a reference material every ~6 measurements. External uncertainty in $\delta^{34}S$ (spot-to-spot reproducibility; 2 standard deviations, noted 2SD hereafter) in CB1 analyses was typically better than 0.5 ‰. The total uncertainty reported on the samples (2σ) is a combination of two independent parameters: (a) the reproducibility of the reference material (CB1) in the respective sessions, and (b) the in-run (measured) uncertainty of the individual analyses. Both (a) and (b) are calculated at the 95 % confidence interval and the uncertainty of each analysis is then calculated as (a) and (b) summed in quadrature.

Sulfur isotopic compositions of pyrites were determined in one analytical session, with analytical conditions close to those for the scapolite measurements: similar primary beam conditions, same counting time and pre-sputtering. The only difference was that a detector with a $10^{10}\Omega$ resistor was used for measurement of ^{32}S, due to the high-count rate of this isotope in pyrite (> 10^9 counts per second). Reference materials Ruttan and Sierra were analyzed alongside the pyrites (Crowe and Vaughan, 1996; Laflamme et al., 2016). All analyses of unknowns were normalized to Ruttan pyrite. All reference materials yielded similar IMF, of ~1.6 ‰, with an accuracy of 0.2 ‰. Reproducibility of the running reference material was better than 0.3 ‰ 2SD. Apatites were also measured in four samples (DK37, Alg-1, CB2, F4812D2), in a separate session (June 19, 2021), following the method and using reference material described in Hammerli et al. (2021). For apatite S isotope analyses all unknowns were normalized to Durango-A ($\delta^{34}S_{VCDT}$ = -1.06 ‰; Hammerli et al. (2021). No drift corrections were applied, except in the session on June 19, 2021, where a linear drift correction was implemented.

4. Sample Petrography

4.1. Mafic granulite xenolith 85–106, McBride Province, Queensland, Australia

Sample 85–106 is a mafic granulite xenolith from the McBride Province in Queensland, Australia, which is recognized as the type locality of silvialite (Teertstra et al., 1999). The major mineral assemblage includes clinopyroxene, garnet, plagioclase, amphibole, and scapolite, with minor ilmenite and magnetite (Rudnick and Taylor, 1987). Among these minerals, clinopyroxene accounts for approximately 60–70 % of the rock. Garnet and plagioclase each make up around 10 % of the mineral assemblage, while scapolite and hornblende are estimated to be present at roughly 5 % each. Scapolite grains, up to 1 mm in diameter with sub- to euhedral shapes, are commonly surrounded by alteration rims measuring 100 to 200 μm in width (Fig. 1 A,B). Scapolite is present as inclusions within clinopyroxene, amphibole and plagioclase, and it also occurs at triple junctions (Fig. 1 A,B). The estimated equilibration temperature for this sample falls within the range of 890 to 1070 °C, as reported in Rudnick and Taylor (1987). This sample is devoid of sulfide minerals.

4.2. Mafic granulite xenolith 1636, Slave craton, Canada

This mafic granulite xenolith (1636) was transported to the surface by a kimberlite in the central Slave craton, Canada (Aulbach et al., 2010). It is suggested to derive from basaltic source rocks, possibly representing subducted oceanic crust or basaltic magma that crystallized near the Moho. It consists of clinopyroxene, garnet, plagioclase, scapolite, with minor rutile, ilmenite, pyrrhotite and accessory apatite (Fig. 1C and 2A). Estimated modal abundances for clinopyroxene and garnet are ~45 % each, followed by scapolite and plagioclase (~5 % each). The scapolite grains are up to 2 mm in size and exhibit subeuhedral to euhedral shapes (Fig. 1C), with some grains displaying alteration rims. Tiny needle-shaped sulfide inclusions with a parallel orientation along cleavage are common in the scapolite. Such inclusions have previously been interpreted as magmatic phases formed coeval with scapolite (Korinevsky and Korinevsky (2016), however, it is also possible that these needles formed as a result of exsolution processes. Thermobarometry on this sample revealed P-T conditions of ~810 °C and ~1.05 GPa (Chacko, unpublished).

4.3. Mafic granulite xenoliths 89–726 and 89–729, Lashaine, Tanzania

Samples 89–726 and 89–729 are mafic garnet-clinopyroxene granulites, which were collected from the Quaternary Lashaine tuff cone within the Mozambique belt (as detailed in Mansur et al., 2014). Sample 89–726 contains ~50 % plagioclase, followed by clinopyroxene (~30

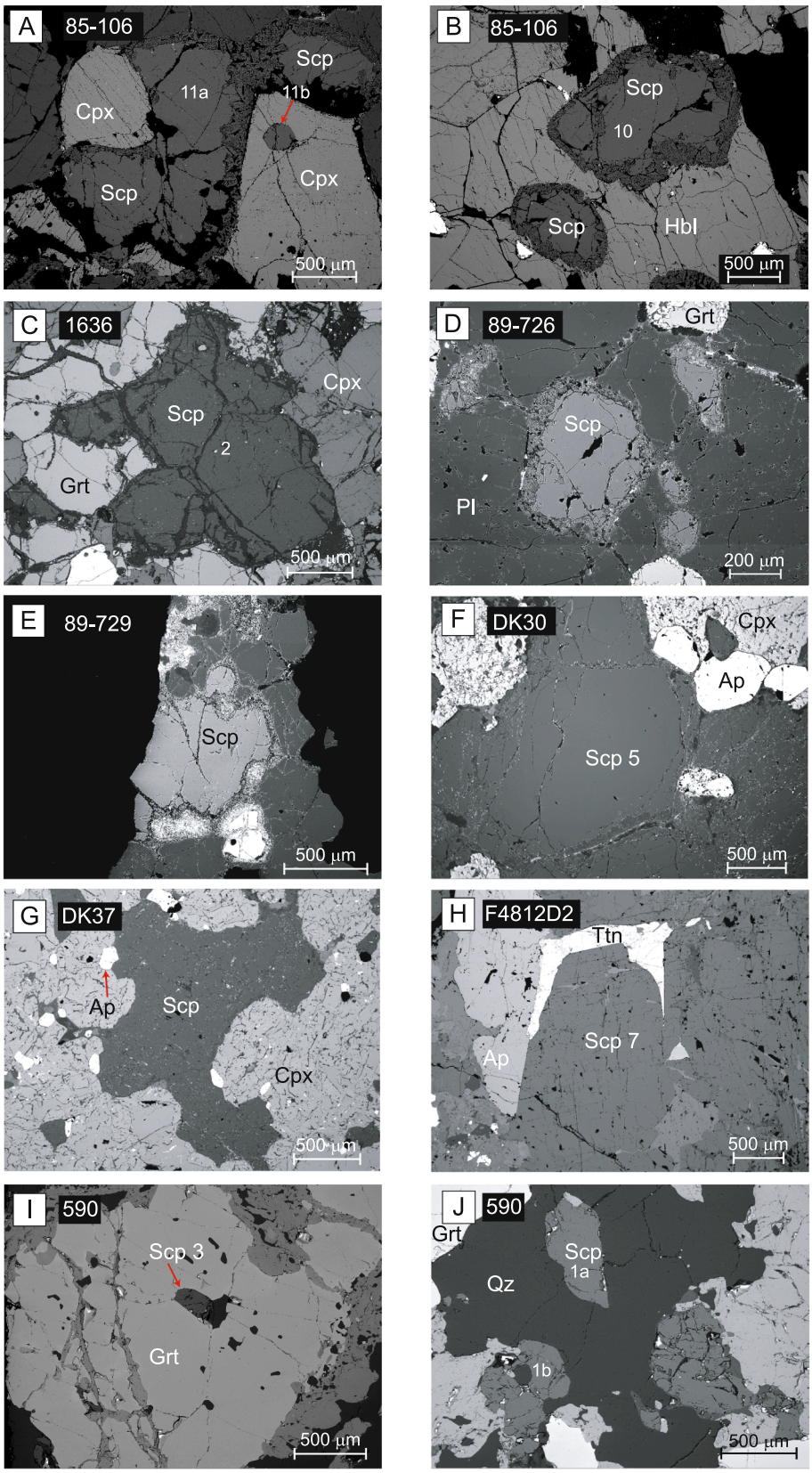

Fig. 1. Representative back-scattered electron (BSE) images of the scapolite-bearing samples investigated in this study. Mineral abbreviations follow Whitney and Evans (2010): Scp = Scapolite, Qz = quartz, Pl = Plagioclase, Ap = Apatite, Cpx = Clinopyroxene, Ttn = titanite, and Hbl = Hornblende. The numbers refer to the analyzed minerals.

%), garnet (~15 %), and scapolite (~5 %). Garnet contains small (~ 10 μm) inclusions of quartz. Scapolite minerals in sample 89–726 reach a maximum size of 1 mm and are (sub-) euhedral in shape (Fig. 1D). This sample also contains minor amounts of apatite, corundum, kyanite, rutile, sulfides, and titanite (Mansur et al., 2014). The sulfides in this sample occur as oval to round inclusions in major minerals including scapolite. These inclusions consist of pentlandite, chalcopyrite, and pyrrhotite (Fig. 2 B,C). Like 89–726, sample 89–729 mainly comprises plagioclase, clinopyroxene and garnet, with accessory scapolite, rutile and titanite (Mansur et al., 2014; Apen et al., 2020). No estimates of modal abundances are provided, since sample 89–729 was analyzed in a grain mount and not in a thin section. The scapolite minerals found in sample 89–729 typically exhibit a subhedral shape and can reach sizes of up to 2 mm (Fig. 1E). Scapolite in both samples have alteration rims, ranging from 50 to 100 μm in width (Fig. 1D, E). Mansur et al. (2014) estimate a peak temperature of 840 °C at 1 GPa for sample 89–729.

4.4. *Pyroxenite xenoliths DK30 and DK37 from SE Pamir of Tajikistan*

Two samples from the Pamir xenolith suite were investigated. Sample DK30 contains pyroxene as its major mineral (~60 %), followed by scapolite (~30 %). Magnetite, titanite, K-feldspar, and apatite are present as minor minerals (~5%). Scapolite grains are up to 2 mm in size and are subhedral; apatite is subhedral to euhedral in shape and reaches 1 mm. Sample DK37 has a similar mineralogy to DK30, with scapolite commonly forming interstitial anhedral grains of up to 2 mm in size (Fig. 1 F,G). However, DK30 differs in that it also includes approximately 5 % K-feldspar. Both samples contain sulfides comprising pyrrhotite and pyrite as well as smaller amounts of chalcopyrite. Sulfides occur at grain boundaries or as round "blobs" (roundish inclusions) in major minerals. Magnetite is interspersed in the sulfides or rims sulfides in some cases (Fig. 2 D-H). Major-element thermobarometry, pseudosections, and oxygen-isotope thermometry indicate that the granulite-facies xenoliths from this suite reached temperatures of ~875–1000 °C and pressures of ~1.8–2.3 GPa (Shaffer et al., 2017).

4.5. *Calc-silicate gneiss F4812D2 from the HT Ikalamavony domain from southern Madagascar*

Sample F4812D2 is a calc-silicate gneiss, characterized by a heterogeneous distribution of minerals, posing challenges in accurately estimating representative modal abundances. The mineralogy comprises clinopyroxene, plagioclase, scapolite, quartz, amphibole, and titanite, with scapolite accounting for approximately 10 % of the bulk rock. Calcite, epidote, garnet, magnetite and apatite are minor phases. Scapolite grains can reach 1 mm in size and are typically euhedral in shape (Fig. 1H). Euhedral apatite can reach 500 μm. No sulfides were found in this sample. Estimated P-T conditions for this sample are 0.4–0.8 GPa at 750–800 °C (Holder and Hacker, 2019).

4.6. *Clinopyroxene- garnet-plagioclase-quartz granulite (590), Western Australia*

This sample comes from an exposure along the Fraser Fault, Western

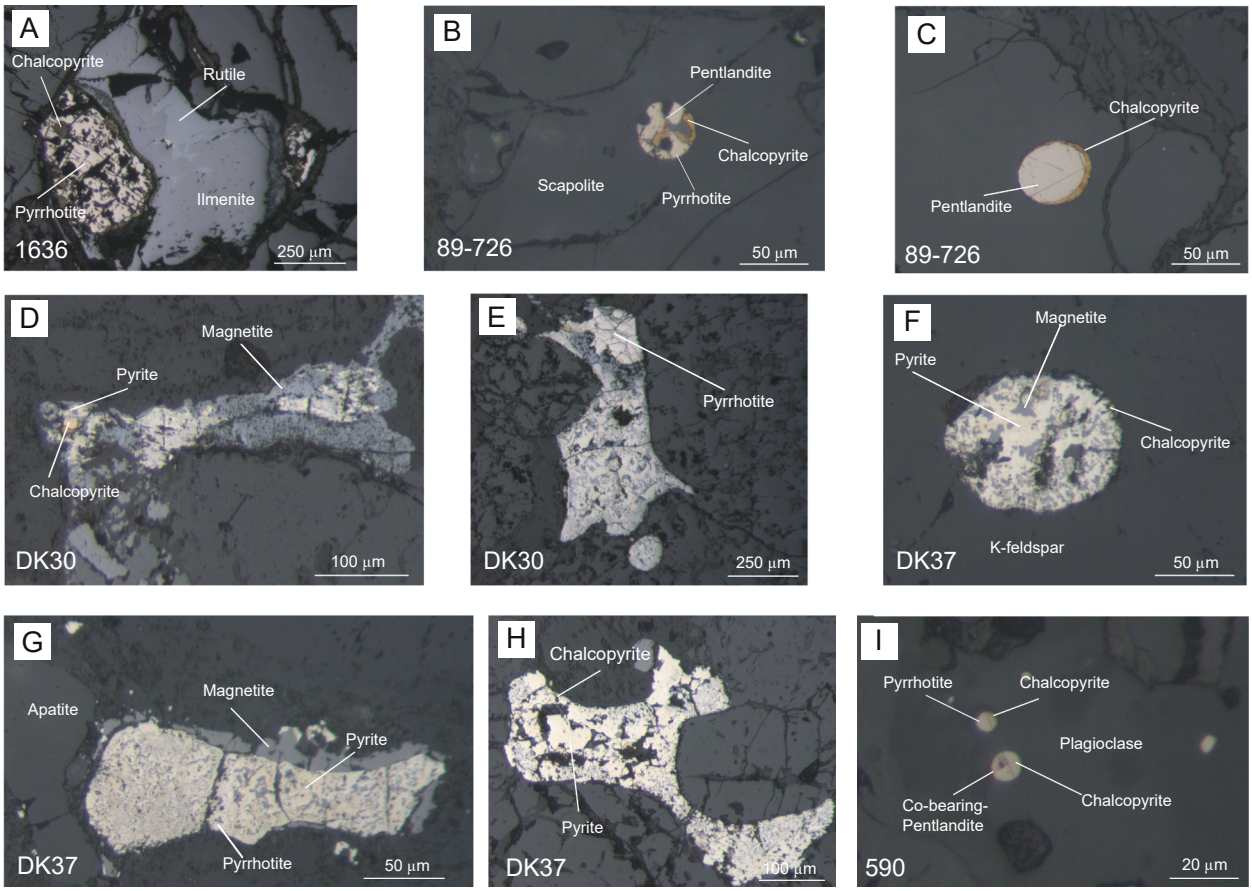

Fig. 2. Representative reflected light photomicrographs of sulfides and oxides in the scapolite-bearing samples. **A)** Pyrrhotite and minor chalcopyrite in Slave craton mafic granulite xenolith 1636 surrounded by ilmenite and rutile. **B)** Complex sulfide inclusion in scapolite of Tanzanian mafic granulite xenolith 89–726 consisting of pyrrhotite, pentlandite, and chalcopyrite. **C)** Pentlandite inclusion with a thin chalcopyrite rim in 89–726. **D) & E)** Typical sulfide and oxide mineral assemblage and textural relationship observed in Pamir pyroxenite xenolith DK30. **F)** "Blob" in K-feldspar consisting of pyrite, magnetite and minor chalcopyrite in Pamir pyroxenite xenolith DK37. **G)** Pyrrhotite and pyrite rimmed by magnetite in DK37. **H)** Typical interstitial sulfide observed in sample DK37. **I)** Sulfide inclusions in Fraser Range mafic granulite 590. Some of the pentlandite grains contain elevated Co contents as detected in EDS measurements.

Australia (sample 90 in Wilson, 1976). Sample 590 is composed of ~40 % clinopyroxene, ~40 % garnet, ~10 % plagioclase, ~5 % quartz and ~5 % scapolite. Scapolite can reach up to 1 mm in size and is typically anhedral; it is present in the matrix as well as being enclosed in major minerals, such as garnets (Fig. 1 I,J). Sulfide inclusions in major minerals, such as plagioclase or pyroxene, are chalcopyrite, pyrrhotite, and Co-bearing pentlandite (Fig. 2 I). These multi-phase inclusions are typically smaller than 20 μm in size. Estimated equilibration temperature for this sample is ~870–890 °C (Goldsmith and Newton, 1977, and references therein).

4.7. Scapolite phenocrysts from Segueika volcano, Algeria and from the Enval-Volvic volcanic line in France

Scapolite Alg-1 (IGSN collection number CNRS0000027719 Atakor, curated at Université Clermont Auvergne) is from the Segueika volcano in Atakor, Algeria. This cinder cone contains a range of minerals, such as kaersutite, oligoclase, titanomagnetite, clinopyroxene and scapolite (Boivin and Camus, 1981). The scapolite studied here is ~5 mm in size, has a grey color and contains apatite inclusions, which are a few hundred μm in size. Scapolite CB2 (IGSN collection number CNRS0000027747 Bannière 3) comes from the Enval-Volvic volcanic line, east of the Chaîne des Puys in the Massif Central, France (the same location as the scapolite standard reference material CB1; see Hammerli et al., 2017). It is a gray, ~ 7 mm crystal and with an alteration rim that is several hundreds of μm wide. Both samples are found in tephra and are thought to represent high-pressure phenocrysts formed at > 10 kbar in the upper mantle (Boivin and Camus, 1981).

5. Results

5.1. Major-element composition of scapolite and apatite

EPMA spot analyses were made across several minerals in each sample to see if compositional differences exist. Representative EPMA analyses of scapolite and average apatite compositions are given in Table 1 and 2, respectively. We also acquired semi-quantitative EPMA maps for a representative scapolite grain in each sample and these maps are also provided in the supplements (Fig. S1). CO_2 concentrations in scapolite are calculated by assuming that the crystal's A-site is full and equals 1 (A = 1 = (S + Cl + C) (see Teertstra et al., 1999 for details). Following Teertstra and Sherriff (1997), the average meionite (Me%) component is expressed as Me% = 100[∑(divalent cations)/4)]. The atomic occupancy of S at the anion site is expressed as X_S from now onward.

5.1.1. Mafic granulite xenolith 85–106, McBride Province, Queensland, Australia

Sample 85–106 contains scapolite with homogeneous major element concentrations. Twenty-six analyses were carried out on a total of 9 grains and the average SO_3 concentration is 5.22 wt% ± 0.31 (2SD), which translates to $X_S = 0.6$. Chlorine concentrations are below the limit of detection (~120 ppm) and calculated CO_2 contents are, on average, 1.80 wt% ± 0.16 (2SD). The average meionite (Me%) component is 72.8 ± 1.2 %, which further shows the compositional homogeneity of scapolite in this sample.

5.1.2. Mafic granulite xenolith 1636, Slave craton, Canada

We conducted 99 EPMA spot analyses on 11 different grains demonstrating that scapolite has a relatively homogeneous composition with only small compositional variations within individual grains. The average SO_3 content is 5.16 wt% ± 0.50 (2SD) and variations within individual grains are typically < 0.5 wt%. Chlorine is present in low concentrations (average = 0.12 wt% ± 0.06) and calculated CO_2 contents are on average 1.77 wt% ± 0.25. The average Me% is 65.6 ± 2.8 and the average X_S is 0.6 ± 0.06. Four apatite grains were analyzed with a total of 16 spot analyses. The SO_3 content of apatite ranges from 0.08 to 0.28 wt%, with this variation primarily observed between individual grains. The most important anion occupying the "channel" site is F with X_F 0.91 ± 0.07.

5.1.3. Mafic granulite xenoliths 89–729 Lashaine, Tanzania

We carried out 29 analyses on 5 different grains. Sulfur concentrations vary significantly between and within the different grains. For example: one of the analysed grains is SO_3-depleted (<400 ppm) while another scapolite contains a maximum amount of 5.16 wt% SO_3. Some grains show internal variations with rims generally being depleted in sulfur compared to cores. Chlorine concentrations are low and typically

Table 1
Representative EPMA analysis of scapolite for each sample. The number of ions is determined on the basis of 12 (Si, Al) and CO_2 is calculated on the assumption that the A-site is fully occupied by C, S and Cl, hence C = 1–S–Cl.

	85-106_3	1636-1A-1	89-729_6_2	89-726_2a_1	DK30_5_6	DK37_1_1	F4812D2_7_2	590-2A-3	Alg-1_14	CB2_2
SiO_2 (wt%)	45.18	48.75	46.46	47.29	48.93	48.06	45.86	48.50	46.33	44.36
Al_2O_3	26.30	24.70	25.94	25.13	24.11	24.92	27.01	25.86	25.91	26.58
FeO	0.27	0.07	0.04	0.12	0.26	0.50	0.27	0.05	0.36	0.47
CaO	17.61	15.82	17.27	16.16	14.33	14.83	18.47	17.05	16.90	18.01
MnO	<0.01	<0.01	<0.01	<0.01	0.04	<0.01	<0.01	<0.01	<0.01	0.02
MgO	0.10	0.02	0.03	0.11	0.03	0.06	0.05	<0.01	0.03	0.12
Na_2O	3.55	4.83	4.01	4.48	5.10	4.93	3.23	4.56	3.99	3.19
K_2O	0.05	0.15	0.08	0.21	0.72	0.61	0.07	<0.01	0.19	0.19
Cl	<0.01	0.15	0.01	0.13	0.33	0.43	0.03	0.08	0.25	0.13
SO_3	5.19	4.95	3.94	4.07	4.84	3.69	2.49	3.33	2.33	4.17
CO_2 (calc.)	1.80	1.84	2.52	2.30	1.65	2.17	3.34	2.89	3.10	2.17
Total	100.05	99.44	100.31	100.00	100.34	100.19	100.82	99.43	99.39	99.42
–O = Cl	<0.01	0.03	<0.01	0.03	0.07	0.10	0.01	0.02	0.06	0.03
Total	100.05	99.40	100.30	99.97	100.27	100.10	100.82	99.41	99.33	99.39
Si (APFU)	7.12	7.51	7.24	7.38	7.59	7.45	7.08	7.37	7.23	7.03
Al	4.88	4.49	4.76	4.62	4.41	4.55	4.92	4.63	4.77	4.97
Fe	0.04	0.01	0.01	0.02	0.03	0.06	0.04	0.01	0.05	0.06
Ca	2.97	2.61	2.88	2.70	2.38	2.46	3.06	2.78	2.83	3.06
Mn	<0.01	<0.01	<0.01	<0.01	<0.01	<0.01	<0.01	<0.01	<0.01	<0.01
Mg	0.02	<0.01	0.01	0.03	0.01	0.01	0.01	<0.01	0.01	0.03
Na	1.08	1.44	1.21	1.36	1.53	1.48	0.97	1.34	1.21	0.98
K	0.01	0.03	0.02	0.04	0.14	0.12	0.01	<0.01	0.04	0.04
Cl	<0.01	0.04	<0.01	0.03	0.09	0.11	0.01	0.02	0.07	0.03
S	0.61	0.57	0.46	0.48	0.56	0.43	0.29	0.38	0.27	0.50
C	0.39	0.39	0.54	0.49	0.35	0.46	0.70	0.60	0.66	0.47

Table 2
Average values and 2SD uncertainties of EPMA analyses of apatite. The stoichiometries are calculated following the method of Ketcham (2015). No CO_2 data were collected and therefore the OH content was calculated assuming that the anion site is filled with F, Cl, and OH.

	1636		DK30		DK37		F4812D2		Alg-1	
	(n = 16)	2SD	(n = 51)	2SD	(n = 74)	2SD	(n = 45)	2SD	(n = 15)	2SD
CaO	54.62	0.87	52.91	0.83	52.30	0.68	55.16	0.52	52.32	0.58
P_2O_5	41.96	0.89	40.49	0.70	40.11	0.82	42.72	0.55	40.05	0.48
SiO_2	0.09	0.07	0.45	0.05	0.50	0.13	0.12	0.09	0.57	0.08
Na_2O	0.08	0.08	0.37	0.06	0.32	0.10	0.02	0.02	0.49	0.08
MgO	0.04	0.05	0.09	0.05	0.06	0.04	<0.01	0.01	0.08	0.02
FeO	0.11	0.13	0.19	0.12	0.20	0.18	0.02	0.22	0.23	0.07
MnO	0.01	0.02	0.05	0.04	0.07	0.05	0.09	0.03	0.15	0.04
SrO	0.10	0.07	0.74	0.08	0.82	0.08	<0.01	<0.01	0.45	0.04
Ce_2O_3	0.24	0.12	0.46	0.13	0.52	0.15	0.04	0.07	0.36	0.12
SO_3	0.14	0.13	0.85	0.07	0.69	0.26	0.13	0.09	0.91	0.14
F	3.42	0.27	2.88	0.24	2.68	0.18	2.39	0.21	1.07	0.10
Cl	0.18	0.11	0.31	0.14	0.29	0.08	0.04	0.02	0.56	0.05
OH calc.	0.21	0.26	0.59	0.18	0.74	0.17	1.24	0.19	2.07	0.11
Total*	99.71	1.23	99.10	1.43	98.10	1.23	100.95	0.71	98.72	0.90
*X*F	0.91	0.07	0.78	0.07	0.73	0.05	0.63	0.06	0.29	0.03
*X*Cl	0.03	0.02	0.04	0.02	0.04	0.01	0.01	0.00	0.08	0.01
*X*OH	0.06	0.08	0.18	0.05	0.23	0.05	0.37	0.06	0.63	0.03

* Corrected for –O=F, Cl.

below the detection limit of ~120 ppm. As in the other samples, the calculated CO_2 concentrations correlate negatively with SO_3 contents, with the lowest value being 1.82 wt% and the highest 4.76 wt%. Compared to CO_2 and SO_3, the other major elements are relatively uniform (see Table 1 and supplementary material), which is reflected by the average Me% of 71.9 ± 2.5 (2SD).

5.1.4. Mafic granulite xenoliths 89–726 Lashaine, Tanzania

A total of 39 analyses of 9 different grains were carried out. The average SO_3 content is 3.97 wt% ± 0.92 (2SD). The lowest measured value is 2.52 wt% and the highest concentration is 4.75 wt%. Some grains contain variable SO_3 contents without that any systematic zoning pattern can while others have homogeneous SO_3 concentrations. The average Cl content is 0.14 wt% ± 0.04 and the average calculated CO_2 concentration is 2.39 wt% ± 0.48. The CO_2 and SO_3 contents are negatively correlated, however, the other major elements have relatively uniform concentrations, which is expressed by the small 2SD value of the average Me% (66.5 ± 1.4). The average X_S is 0.46 ± 0.11 (2SD) and X_C is 0.50 ± 0.11 (2SD).

5.1.5. Pyroxenite xenolith DK30 from SE Pamir of Tajikistan

Scapolite in sample DK30 is homogeneous; 28 analyses of 6 different grains do not show any chemical zonation. The average SO_3 content is 4.87 wt% ± 0.19 (2SD) and the average chlorine concentration is 0.07 wt% ± 0.02 (2SD). The average calculated CO_2 content is 1.73 wt% ± 0.14 (2SD) and Me% is 59.8 ± 1.2 (2SD) further emphasizing the homogeneity of major element concentrations. The atomic occupancy for S at the A-site is on average 0.56. Four apatite grains were analyzed and 52 spot analyses along different transects of the individual grains indicate that the grains are chemical homogeneous (Table 2). The average SO_3 content is 0.85 wt% ± 0.07 (2SD) and the most important anion occupying the "channel" site is F with X_F 0.78 ± 0.07.

5.1.6. Pyroxenite xenolith DK37 from SE Pamir of Tajikistan

We conducted 31 analyses on 5 different scapolite grains and found that SO_3 concentrations vary between 2.89 and 4.31 wt%. Maximum variation within the same grain is ~1 wt% and there seems to be no correlation between potential growth zones or other microstructural features. However, most grains contain relatively homogeneous SO_3 concentrations resulting in an average of 3.41 wt% ± 0.56 (2SD). Chlorine concentrations are low and vary minimally and return an average of 0.44 ± 0.04 (2SD) wt. %. Stoichiometrically determined CO_2 concentrations mirror the variations of the SO_3 contents and vary from 1.63 to 2.65 wt%. The average Me% is 62.3 ± 1.8 (2SD). CO_3^{2-} is the most important component in the A-site (X_C 0.48 ± 0.07), followed by SO_4^{2-} (X_S = 0.40 ± 0.07). Twelve apatite grains were analyzed with a total of 75 spot analyses. The SO_3 content of apatite ranges from 0.4 to 0.9 wt%. Some grains show compositional zoning in which rims have elevated sulfur concentrations compared to internal zones (e.g., ~0.75 wt% SO_3 vs. 0.44 wt% SO_3). However, these zones are not discernible in BSE images. As for sample DK30, fluorine is the most important anion in the crystal's channel site (X_F = 0.73 ± 0.05 (2SD)).

5.1.7. Madagascar calc-silicate gneiss F4812D2

A total of 35 spots were analyzed on 5 different grains. Large variations in SO_3 contents between the analyzed grains as well as within individual grains are evident. The highest SO_3 concentration of 3.3 wt% was measured in rims of a highly zoned crystal (Fig. 4). The same crystal contains a "core" zone with low SO_3 concentrations (~1.4 wt%). One of the analyzed grains contains low, but homogenous SO_3 concentrations of ~0.5 wt%. Similar to the other samples, chlorine is present in low concentrations (average = 0.04 wt% ± 0.01 (2SD), and CO_2 contents are negatively correlated with SO_3 contents; the lowest calculated value is 2.85 wt% and the highest is 4.45 wt%. Other major elements do not show significant variations and the average Me% is 75.2 ± 3.2 (2SD). The X_S value is always < 0.5 with an average of 0.21 ± 0.18 (2SD). In addition to scapolite, we analyzed four apatite grains with a total of 45 spot analysis. The average SO_3 content is 0.13 wt% ± 0.09 and some grains show compositional variations that range within individual grains from 0.07 to 0.21 wt%. Fluorine occupies most of the "channel" site of apatite with X_F = 0.63 ± 0.06 (2SD) (Table 2).

5.1.8. Clinopyroxene- garnet-plagioclase-quartz granulite (590), Western Australia

A total of 104 spots were analysed in 13 different grains. The average SO_3 concentration is 3.30 wt% ± 0.67 (2SD). The highest value measured is 4.2 wt% and the lowest 2.1 wt% SO_3. SO_3 contents in individual grains can vary by up to 1.5 wt%, however, no distinct zoning is observed. Chlorine concentrations are low (average = 0.08 ± 0.05 (2SD)) and the average calculated CO_2 content is 2.88 wt% ± 0.36 (2SD). As observed in the other samples, major elements such as Na, Ca, and Si have very similar concentrations in the different grains, which results in an Me% of 67.2 ± 1.6 (2SD). The average X_S is 0.38 ± 0.08 (2SD) and the average X_C is 0.60 ± 0.07 (2SD).

5.1.9. Scapolite xenocrysts Alg-1 from Algeria and CB2 from the Massif Central, France

We analyzed one transect (n = 16) across a large Alg-1 scapolite crystal. The results show that the grain is homogeneous with an average SO_3 content of 2.31 wt% ± 0.12 (2SD) and an average Cl concentration of 0.25 wt% ± 0.02. Stoichiometrically constrained CO_2 contents average 3.09 wt% ± 0.09. The grain's Me% is 69.6 ± 1.4 (2SD) and X_S is 0.27 ± 0.02 (2SD). Three apatite grains present as inclusions in the scapolite were analyzed (n = 16) for their major element composition by EPMA. Apatite grains are homogeneous in their compositions and contain between ~0.8 and ~1 wt% SO_3 with an average content of 0.91 ± 0.14 (2SD). In the absence of CO_2-data and under the assumption that Cl, F, and OH fill the anion sites, the results show that OH (X_{OH} = 0.63 ± 0.03 (2SD)) occupies most of these sites (Table 2). Four EPMA analyses of scapolite CB2 returned an average of 4.14 wt% ± 0.11 (2SD) for SO_3, 0.13 wt% ± 0.01 (2SD) Cl, and an average of 2.18 wt% ± 0.08 (2SD) for CO_2. The Me% is 75.75 ± 0.84 (2SD) and X_S is 0.49 ± 0.01 (2SD).

5.2. Sulfur isotopes

5.2.1. Whole grain fluorination

Two Alg-1 aliquots returned $\delta^{34}S$ values of 6.94 ‰ ± 0.30 (2SD) and 6.30 ‰ ± 0.30 (2SD), with mass-dependent $\Delta^{33}S$ (−0.014 ‰ ± 0.016; −0.022 ‰ ± 0.016) and $\Delta^{36}S$ values (0.28 ‰ ± 0.30; 0.07 ‰ ± 0.30). Two analyses of CB2 material yielded $\delta^{34}S$ values of 4.94 ‰ ± 0.30 (2SD) and 4.54 ‰ ± 0.30 (2SD), with mass-dependent $\Delta^{33}S$ (0.002 ‰ ± 0.016; −0.020 ‰ ± 0.016) and $\Delta^{36}S$ values (0.10 ‰ ± 0.30; −0.16 ‰ ± 0.30). Uncertainties in the $\delta^{33}S$ and $\delta^{36}S$ values for Alg-1 and CB2 correlate strongly with the uncertainties for $\delta^{34}S$ values due to mass-dependent fractionation processes in the measurement procedure (cf. Wing and Farquhar, 2015), giving rise to significant statistical covariances among the uncertainties in these measurements.

5.2.2. New scapolite secondary standards CB2 and Alg-1 for SIMS S isotope analysis

SIMS sulfur isotope analyses of the two scapolites Alg-1 and CB2 that were characterized for their isotope signatures via the fluorination method are shown in Fig. 3. By using CB1 (Hammerli et al., 2017) to normalize SIMS measurements of Alg-1 and CB2 (i.e., treating Alg-1 and CB2 as unknowns), individual SIMS analyses are in good agreement with the whole grain values. The mean $\delta^{34}S$ value of Alg-1 measured by SIMS is 6.1 ± 0.9 ‰ (2SD), which is within the uncertainty of the average whole grain value of 6.6 ± 0.9 ‰ (2SD). However, the bulk grain value consists of two analyses only due to the limited amount of available sample material. Scapolite CB2 returned an average SIMS $\delta^{34}S$ value of 4.5 ± 0.4 ‰ (2SD), which is excellent agreement with the average whole grain value of 4.7 ± 0.6 ‰ (2SD) that is also based on two analyses (see above).

5.2.3. Scapolite in granulites

5.2.3.1. Mafic granulite xenolith 85–106, McBride Province, Queensland, Australia. Eight different scapolite grains from the "McBride" xenolith (85–106) were measured in situ for their sulfur isotope compositions. There is no compositional difference (beyond analytical uncertainty) between scapolite located in the matrix or included in other major minerals, such as clinopyroxene (Fig. 4A). The 32 analyses show that there is no $\delta^{34}S$ heterogeneity in the different grains (Fig. 5) and isotope variations along transects in individual grains typically fall within analytical uncertainties. The average $\delta^{34}S$ value of scapolite grains in this sample is −2.5 ± 0.9 ‰ (2SD).

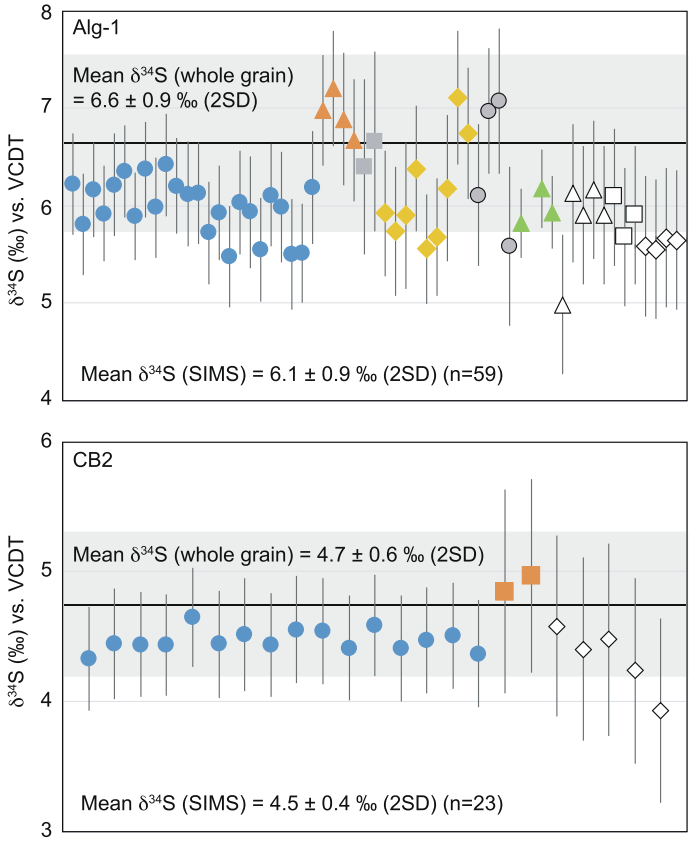

Fig. 3. Compilation of secondary scapolite standards Alg-1 and CB2. Different symbols and colors distinguish different analytical sessions and all data are normalized to the $\delta^{34}S$ value of scapolite CB1 (5.08 ± 0.40 ‰). All uncertainties combine internal uncertainties and the standard deviation of the primary standard CB1 at the 95 % confidence interval.

5.2.3.2. Mafic granulite xenolith 1636, Slave craton, Canada. Sulfur isotope ratios in the analysed scapolite show relatively homogeneous values across individual grains (Fig. 5). A total of 21 analyses in 4 different grains returned an average $\delta^{34}S$ of 2.7 ‰ ± 0.9 (2SD).

5.2.3.3. Mafic granulite xenolith 89–729 Lashaine, Tanzania. Isotope analyses were conducted on four scapolite grains. The $\delta^{34}S$ ratios exhibit a range from −1.5 to 3.6 ‰ within this sample, with individual grains displaying isotope variations of ~3 to 3.5 ‰ (Fig. 5). These variations are evident irrespective of the grain's sulfur content or the presence of cracks. Notably, no correlation between the analysis location and the sulfur isotope ratios was observed.

5.2.3.4. Mafic granulite xenolith 89–726 Lashaine, Tanzania. Nine scapolites were analyzed in 89–726 with a total of 42 individual analyses. Sulfur isotopes ratios range from $\delta^{34}S$ ~−2.5 ‰ to ~+2.2 ‰ (Fig. 5). These variations can be observed between individual grains but also within single grains in some cases, with the inner zones of scapolites containing lower S isotope ratios compared to spots closer to the grain boundary.

5.2.3.5. Pyroxenite xenolith DK30 from SE Pamir of Tajikistan. Sulfur isotope analyses in scapolite from Pamir pyroxenite DK30 show homogeneous isotope ratios (Fig. 5). The average (n = 28) $\delta^{34}S$ value of measurements in eight individual scapolites is 8.8 ± 0.5 ‰ (2SD). In addition to scapolite, we also analyzed sulfur isotopes of five apatite grains with a total of 42 measurements. Analyses along transects show that all apatite are isotopically homogeneous. The average $\delta^{34}S$ (9.0 ± 0.8 ‰ (2SD)) is in excellent agreement with scapolite S isotope measurements. One pyrite grain was analyzed via three individual measurements and sulfur isotope ratios of these analyses range from 4.2 to 4.7 ‰ $\delta^{34}S$ (Fig. 5).

5.2.3.6. Pyroxenite xenolith DK37 from SE Pamir of Tajikistan. Transects of two scapolite grains were analyzed (n = 13). The results show consistent $\delta^{34}S$ values, with all but one analysis returning sulfur isotope ratios that fall within each other's analytical uncertainties (Fig. 5). The average $\delta^{34}S$ value of scapolite in DK37 is 9.4 ± 1.3 ‰ (2SD). We analyzed 8 pyrite grains a total of 19 times, which returned an average $\delta^{34}S$ of 3.8 ‰ ± 0.6 (2SD).

5.2.3.7. Madagascar calc-silicate gneiss F4812D2. Sample F4812D2 contains scapolite with the most distinct compositional zoning (see section 5.1.7 and Fig. 4B). Sulfur isotope ratios measured in different zones (Fig. 5, and Fig. 4B) vary significantly. The core of the grain, with the lowest S concentration, has $\delta^{34}S$ values of −0.70 to −1.10 ‰, followed by a zone with $\delta^{34}S$ of 0.03 to 0.68 ‰. Zones with the highest S content show the highest S isotope ratios (2.15–3.37 ‰ $\delta^{34}S$) (Fig. 4B). Other scapolites measured in this sample contain $\delta^{34}S$ that are similar to the different zones found in grain 7 (Fig. 5), however, not all grains show internal zoning. In addition to scapolite, we also measured S isotopes in two large apatite grains via analytical transects with a total of 16 measurements. These transects also show internal isotope variations of ~2.5 ‰ $\delta^{34}S$. The lowest value is −1.3 ‰, while the highest value is +1.3 ‰, with the inner zones of the apatite exhibiting the higher values.

5.2.3.8. Clinopyroxene-garnet-plagioclase-quartz granulite (590), Western Australia. We analyzed seven scapolite grains, with a total of 31 individual measurements. Some grains exhibit a uniform isotope composition along transects, whereas other grains show isotope ratio variability beyond analytical uncertainty. The highest S isotope values reach 6.6 ‰ $\delta^{34}S$, while the lowest value is 2 ‰. The highest and lowest values occur in different grains, and the maximum variability within a single measured grain is ~2 ‰ (Fig. 5).

5.2.3.9. Scapolite xenocrysts Alg-1 from Algeria and CB2 from the Massif Central, France. The results for these two crystals are given in section 5.2.2. In addition, Alg-1 also contained apatite inclusions within the scapolite, which are homogeneous in their S isotope composition. Twelve analyses in 3 different grains returned a $\delta^{34}S$ value of 5.8 ± 0.7 ‰ (2SD), which is almost identical to the S isotope values of the scapolite host (see Fig. 5).

6. Discussion

6.1. Formation of S-rich scapolite in the lower crust

Understanding the formation of scapolite in lower crustal rocks is crucial for gaining insights into volatile transfer processes, whether from the mantle to the crust or from the surface to the lower crust and back, the latter in the case of granulites with metasedimentary protoliths. In general, the formation of S- and C-rich scapolite in granulites can be attributed to four different scenarios, which are discussed in detail by Moecher et al. (1994) and Hammerli et al. (2017): 1) S and C are transported in their protolith to the lower crust via tectonic/burial processes where the stability field of S- and C-rich scapolite is reached,

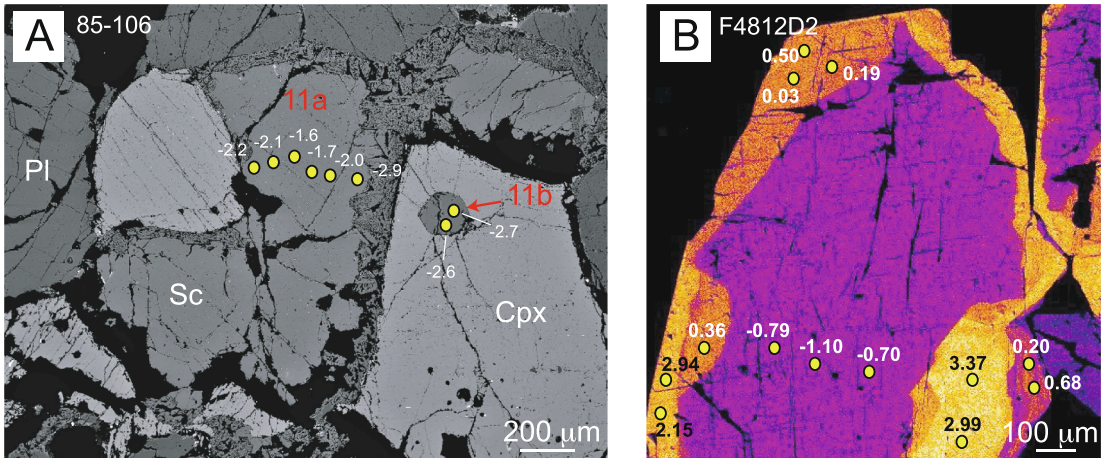

Fig. 4. A) BSE image of location of analytical spots for SIMS measurements in mafic granulite xenolith 85–106 scapolite (grain 11a) and a euhedral scapolite grain enclosed in clinopyroxene (grain 11b). B) A semi-quantitative WDS map of compositionally zoned scapolite grain 7 in Madagascar granulite F4812D2 in which brighter colors indicate a higher S content. Sulfur isotope values ($\delta^{34}S$ ‰) are shown as white (and black) numbers whose typical uncertainties are 0.6 ‰ in sample 85–106 and ≤0.5 ‰ in sample F4812D2 at the 95 % confidence interval.

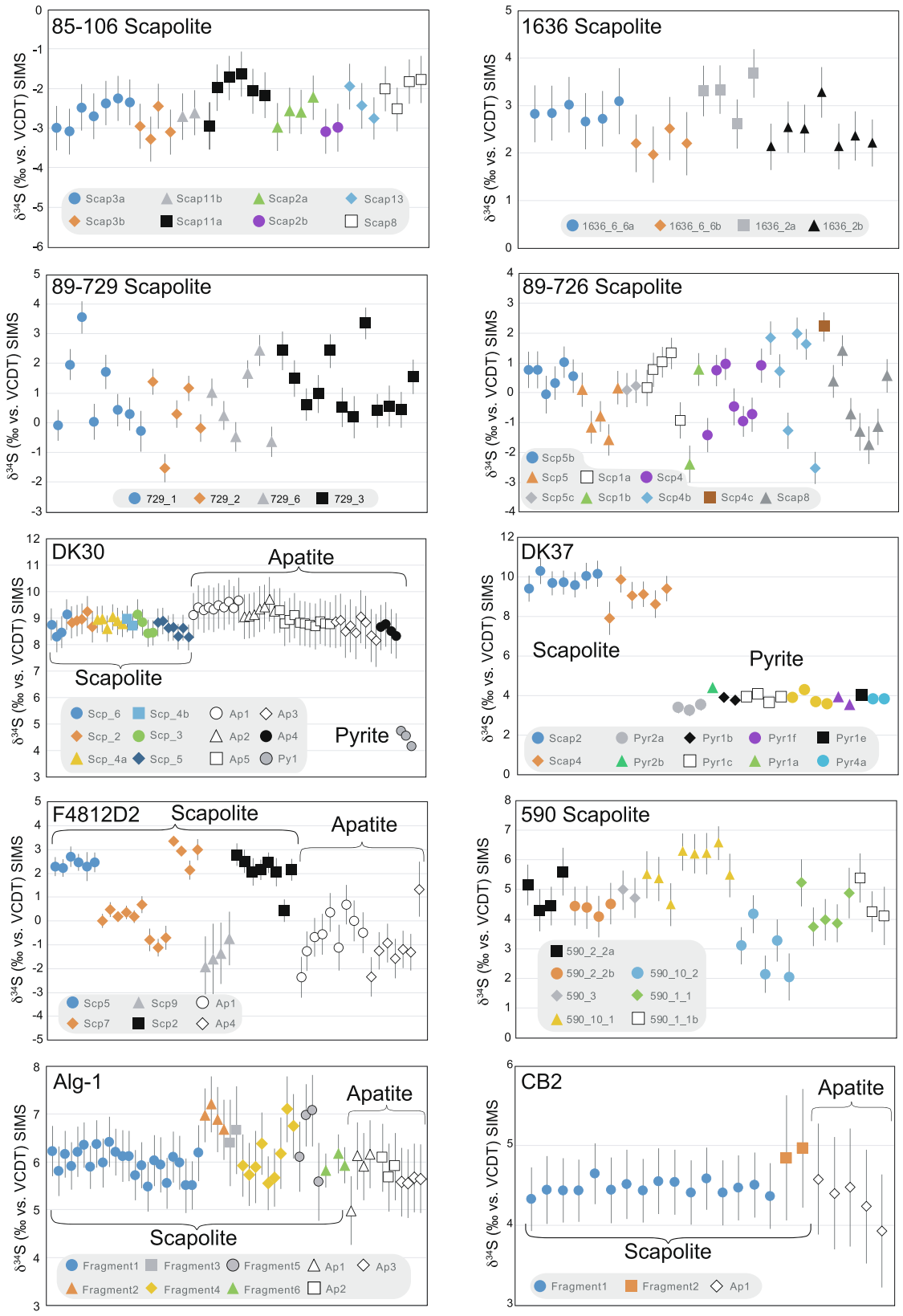

Fig. 5. Sulfur isotope ratios of scapolite, apatite, and pyrite from the studied samples. Each analysed grain is show in a different color with multiple analytical spots. Uncertainties are at the 95% confidence level.

2) scapolite crystallizes as a primary magmatic phase, 3) scapolite formation is triggered by the influx of an external S- and C-rich fluid/melt into the lower crust (i.e., it is metasomatic), 4) scapolite forms in the lower crust when primary S-bearing phases (e.g., sulfides) and silicates present in lower crustal rocks react with CO_2-bearing fluids exsolved from mantle-derived mafic melts.

Analyzing the textural relationships between scapolite and other major minerals in the rock, as well as documenting scapolite inclusions within major minerals and the presence of sulfides and oxides, can aid in distinguishing between the different origins described above. Based on this approach, we briefly discuss which of these origins may be the most plausible for each of the studied samples. Following this analysis and prior research, we have categorized our samples as follows: very likely magmatic origin (mafic granulite xenolith 85–106), likely magmatic origin (mafic granulite 590, 89–726, and 89–729), unclear but potentially magmatic (pyroxenite xenoliths DK30 and DK37), unclear (mafic granulite xenolith 1636), and likely metamorphic origin (calc-silicate gneiss F4812D2). Xenocryst CB2 and Alg-1 likely formed as igneous phases in the upper mantle and hence are not included in the above groups. More detailed information on each sample is provided below.

Mafic granulite 85–106, from the McBride Province, Australia has a whole-rock composition indicating its formation as a deep-seated cumulate from a basaltic melt (Rudnick and Taylor, 1987). Stolz (1987) studied scapolite in mafic xenoliths from the McBride Province, Australia and reported well-shaped scapolite inclusions in plagioclase and clinopyroxene, as well as garnet reaction coronas around scapolite grains. Based on compositional banding and P-T calculations Stolz (1987) suggested that scapolite initially crystallized as a primary magmatic phase and later formed igneous cumulates together with other major phases present in the sample. Our observations align with this conclusion, confirming the presence of euhedral scapolite as inclusions in pyroxene (Fig. 4A). The uniform geochemistry and consistent S isotope composition of scapolite in this sample further support an igneous origin (see sections below).

In mafic granulite 590 from Western Australia, scapolite inclusions occur in garnet and crystalized sulfide melt inclusions occur in clinopyroxene. Wilson (1976) proposed that the protoliths of the mafic pyroxene granulites from the Fraser Range are continental tholeiites and associated gabbroic rocks. According to Wilson (1976), one piece of evidence supporting this is the presence of sedimentary bands interlayered with the granulite units. The sulfide inclusions in major minerals suggest that these rocks experienced some degree of melt interaction in the deep crust. Therefore, the scapolite may have formed as an igneous phase.

Only a limited amount of sample material (i.e., a grain mount) was available for the mafic granulite samples 89–729 from Tanzania and hence it is difficult to investigate textural relationships, though texturally and geochemically it is similar to 89–726, which likely formed as an anorthositic cumulate near the base of a double-thickened crust (Mansur et al., 2014 and references therein). It contains euhedral scapolite inclusions in plagioclase, which may also suggest a magmatic origin. The recrystallized sulfide inclusions in scapolite (Fig. 2 B,C) may support the formation of primary scapolite from a melt that contained a separate sulfide melt (see below).

It is unclear how scapolite formed in samples DK30 and DK37 from SE Pamir of Tajikistan. DK30 and DK37 lack euhedral scapolite grains or scapolite inclusions in other major minerals. However, the presence of interstitial scapolite and interstitial sulfides (see Figs. 1 F,G and 2 D-H) may suggest that scapolite is a late-stage igneous phase.

The formation of mafic granulite xenolith 1636 from the Slave Craton, Canada, is difficult to determine. As discussed in Aulbach et al. (2010), this sample could either represent a magmatic rock that was tectonically transported to the lower crust and underwent granulite-facies metamorphism, or it could have formed at the base of the crust, crystallizing from a basaltic magma. In the latter case scapolite could be magmatic but there is no clear textural evidence for such an origin.

Conversely, sample F4812D2 from southern Madagascar, a calc-silicate rock, exhibits euhedral scapolite grains with compositional and isotopic zoning. Considering the rock's composition (calc-silicate) and under the assumption that the rock has a calcareous metasedimentary protolith, a magmatic origin for the scapolite is unlikely. Moreover, the absence of sulfides in this sample hints at their potential consumption during high-grade metamorphic reactions, leading to the formation of S-bearing scapolite.

Scapolite in the two volcanic rocks (CB2 and Alg-1) has previously been suggested to have crystallized from alkalic magmas as high-pressure (>10 kbar) phenocrysts in the upper mantle (Boivin and Camus, 1981). The consistent geochemical compositions and sulfur isotope ratios further support an igneous origin for these grains, indicating that the upper mantle may, at least locally or regionally, be relatively oxidized.

6.2. *Sulfur transfer from the mantle to the lower crust via sulfide-melts and consequences for scapolite formation*

According to Morrissey and Tomkins (2020), it is common to find both sulfides and S-bearing scapolite within the same sample, an association that likely signifies a system stabilized by the equilibration of sulfides and sulfates. Hamisi et al. (2023) demonstrated that scapolite in graphite-bearing samples harbors sulfur in diverse valence states, with the oxidized forms prevalent. This contrasts with previous studies (e.g., Connolly and Cesare, 1993; Tomkins, 2010), which suggested that the presence of graphite regulates fluids to conditions significantly below the sulfate-sulfide boundary. As a result, the study by Hamisi et al. (2023) concluded that the higher abundance of oxidized S species in scapolite, compared to S^{2-} and polysulfides, likely arises from strong crystallographic control influencing the incorporation of oxidized sulfur in some minerals. This suggests that scapolite can stabilize oxidized sulfur even at oxygen fugacities below the sulfide-sulfate boundary. From these studies we infer that most of the sulfur incorporated in the lower-crustal scapolites described here is in its oxidized form and that scapolite, and to a lesser degree apatite, sequester most oxidized sulfur in the lower crust. This inference has potential implications for metal transport upon scapolite breakdown, as discussed below (see section 6.3). Textural evidence, such as interstitial sulfides or recrystallized sulfide melt inclusions, suggests that a sulfide melt phase was in equilibrium with scapolite in some of the samples we studied, where disproportionation of sulfur may play a role. This would also be supported if the sulfide needles in scapolite from mafic granulite 1636 (Fig. S2) were indeed magmatic and formed co-genetically with magmatic scapolite (Korinevsky and Korinevsky, 2016) rather than being a product of subsolidus exsolution. The presence of sulfide melt in the lower crust has been documented in previous studies on natural samples (e.g., Holwell et al., 2022) as well as experimentally (e.g., Wang et al., 2023). Sulfide droplets derived from the mantle, transported to the lower crust with silicate melt in conduit zones, may explain the presence of magmatic sulfide inclusions in granulite-facies rocks (e.g., Wang et al., 2023). Furthermore, Chen et al. (2020) argued that sulfide-bearing cumulates at the crust-mantle boundary might be an important reservoir for metals, such as Cu, which are depleted in the crust. The sulfide assemblages identified in our study (as minute inclusions in major minerals and at grain boundaries) are characteristic of magmatic sulfides, consisting of pyrrhotite, pentlandite, chalcopyrite, and pyrite. These assemblages may have formed from the recrystallization of monosulfide solid solution and intermediate solid solution phases, as detailed by Holwell et al.'s (2022) (see their Fig. 6). When sulfides are introduced to the lower crust, redox reactions, as proposed by Goldsmith (1976) may occur. For instance, plagioclase reacting with magmatic sulfides through the reaction S^{2-} (in sulfide) + $4Fe_2O_3$ (in magnetite or the Fe_2O_3 component in ilmenite) → SO_4^{2-} (in scapolite) + 8FeO (in silicate), could have generated scapolite in some of the samples described in this work where there is no compelling evidence for magmatic scapolite. The presence of magnetite or ilmenite and Fe-bearing silicates would support such a scenario, at least from a mineral assemblage perspective. In cases where sulfides are absent, and scapolite's primary igneous origin is unlikely (e.g., F4812D2), exhaustion of the sulfur source (i.e., sulfur-bearing phases in the protolith) might have been the limiting factor for scapolite formation. The

suggestion that most S in (mafic) granulites is sourced from the mantle is consistent with the conclusions of Moecher et al. (1994), who studied a large suite of CO_3^{2-}- and SO_4^{2-}- rich scapolite in xenoliths and in high-grade metamorphic rock outcrops. They showed that the carbon isotope composition of scapolite in mafic granulites point to a mantle source.

An essential factor in the formation of S-rich scapolite is the absence of high aH_2O fluids. Experimental work by Newton and Goldsmith (1976) demonstrated that even a small amount of H_2O can stabilize zoisite over CO_3^{2-}- and SO_4^{2-}- rich scapolite, labelling it a hydrophobic compound. Additionally, Porter and Austrheim (2017) showed that hydration during amphibolite-facies retrogression can lead to silvialite breakdown. Consequently "aqueous" fluids are unlikely to be present when scapolite forms. It is more likely that when slab-derived fluids infiltrate the overlying mantle wedge, they can both trigger melting and implant sulfur in the wedge peridotite, which later contributes to the formation of immiscible sulfide melts that segregate from a primary silicate melt (e.g., Du et al., 2014). This slab-derived sulfur may ultimately be incorporated into sulfur-bearing scapolite in the lower crust, which can form either during crystallization as a magmatic mineral in mantle-derived melts or when magmatic sulfides react with silicate minerals to produce scapolite during granulite-facies metamorphism. Such volatile-rich metasomatism of the upper mantle is common and has been observed in various settings such as in xenoliths of the intraplate Montpellier volcanic province in France (Alard et al., 2011), and in the East African rift (Chesley et al., 1999).

6.3. Isotope signatures of the lower crust and implications for crustal fluids

Our sulfur isotope analyses of scapolite, apatite, and pyrite show that S sequestered in these minerals can have $\delta^{34}S$ that ranges from approximately −3 to +10 ‰; furthermore, in some samples (e.g., F4812D2, 89–726, 590) significant (up to 5 ‰) isotope variations between and within individual scapolite grains is observed (Fig. 5). Such variations suggest that the samples were not buffered by a homogeneous S-rich fluid and hence only local isotope equilibration was reached. Dottin et al. (2020) showed that sulfide inclusions in phenocrysts within basalts from a single hot-spot (Mengai) have more than a 5 ‰ range in $\delta^{34}S$ (−5.13 to +0.21 ‰) and Cabral et al. (2013) claimed that individual sulfides may vary even more in $\delta^{34}S$. These authors suggest that the variations are due to the entrapment of melt from diverse sources with different S isotope values. Although the S isotope composition of sulfide melt inclusions were not measured in our study, it is conceivable that the various sulfides in our samples are not in isotopic equilibrium. If magmatic sulfides interacted with silicates to form scapolite within a silicate-buffered environment, the sulfur isotope range of the sulfides might be transferred to the scapolite grains, depending on the scale at which isotope equilibration/homogenization occurs. Complete consumption of minute sulfides would eliminate isotope fractionation between the consumed sulfide grains and scapolite. In Pamir pyroxenites DK30 and DK37, where apatite, scapolite, and interstitial sulfides are present, the difference in S isotope compositions between sulfides and scapolite/apatite is approximately 5 ‰, consistent with the expected equilibrium fractionation of S isotopes between sulfides and sulfate at ~900 °C (Miyoshi et al., 1984). However, in cases where it may be assumed that scapolite formed from a melt, such as in mafic granulite

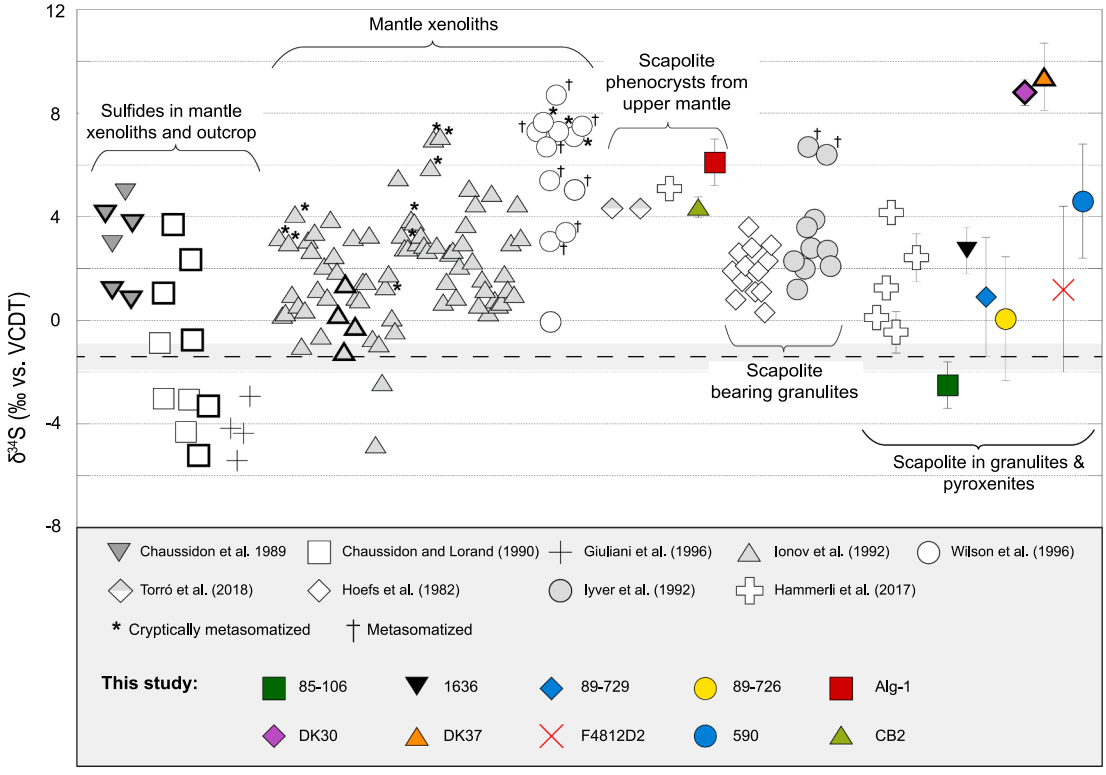

Fig. 6. Compilation of S isotope ratios in sulfides in mantle xenoliths and mantle outcrops (Chaussidon et al., 1989; Chaussidon and Lorand, 1990; Giuliani et al., 2016), whole rock mantle xenoliths and xenocrysts (Ionov et al., 1992; Wilson et al., 1996), scapolite phenocrysts from the upper mantle (Hammerli et al., 2017; Torró et al., 2018), whole rock scapolite-bearing granulites (Hoefs et al., 1982; Iyver et al., 1992), and scapolite in granulites (Hammerli et al., 2017), compared with new scapolite S isotope data from this study. The new data are shown as averages with 2SD uncertainties. For samples where multiple sulfides were measured, the average values are plotted. Symbols with bold outlines represent pyroxenites. * Depicts samples identified by the respective authors as having been affected by cryptic metasomatism, and † denotes samples that are clearly metasomatized. The dotted line represents depleted mantle S isotope ratios after Labidi et al. (2012, 2014), and the grey band shows the 2SD uncertainty.

590, sulfur isotope heterogeneity between individual scapolite grains is more difficult to explain, but may be due to isotopic heterogeneity in the melt mush or Rayleigh fractionation during the crystallization of the melt. Sulfur isotope variation in granulites with a metasedimentary protolith (e.g., F4812D2) might be due to isotope heterogeneity in the protolith itself that was not homogenized before scapolite grew during granulite-faces metamorphism. This example also suggests it is plausible that a range of S isotope signatures can be transferred from the surface to the lower crust.

Our new S isotope data for scapolites overlap with those of the depleted mantle, metasomatized mantle xenoliths, and scapolite formed in the upper mantle (Figs. 6, 7). This suggests that S from (metasomatized) mantle is introduced to the lower crust via, for example, scapolite-bearing melts or sulfide melts, as inferred for the mafic granulites and as discussed in sections 6.1 and 6.2. Furthermore, the presence of S-rich scapolite also implies that S (and C) is stored in the lower crust not only in its reduced forms but also as S^{6+} (and S^{4+}, Hamisi et al., 2023). The common occurrence of scapolite in lower crustal rocks shows that, in addition to both sulfides and sulfates, silicates may regulate the mobility of sulfur from the upper mantle/lower crust to the middle and upper crust. Thus, the mineral assemblage in the lower crust could have a significant impact on the transfer of sulfur from the mantle to the upper crust.

Sulfur liberated from scapolite breakdown may influence the isotopic composition of retrograde metamorphic fluids. Scapolite may release fluids with S isotope compositions resembling the mantle (e.g., mafic granulite 85–106) without the participation of mantle melts during exhumation. Conversely, other samples (e.g., mafic granulite 590) would impart fluids with relatively ^{34}S-enriched sulfur isotope signatures. When some of the S becomes reduced and forms sulfides—such as during the formation of epidote and amphibole containing ferric iron during the breakdown of scapolite (Porter and Austrheim, 2017)—isotope fractionation might lead to higher δ^{34}S values in the residual sulfur in the fluid that did not react to form sulfides.

Vry et al. (2010) and Shulaker et al. (2024) show that significant fluid release may attend exhumation of deep-seated rocks, in tandem with element mobility. Specifically, granulites and their potential to release fluids may be linked to mineralization. Previous work suggests that CO_2-rich fluids (e.g., Touret, 1992) or high salinity, S-bearing fluids result in low aH_2O, which leads to the formation of granulites (e.g., Manning and Aranovich, 2014; Harlov and Hansen 2005; Harlov, 2012; Harlov, 2024 and references therein). In cases where lower crustal rocks are infused with CO_2 during the peak of granulite-facies metamorphism (e.g., Touret, 1992), a substantial portion of high X_{CO2} pore fluid is typically mixed with and replaced by aqueous fluids during exhumation. This "CO_2 dehydration" forms extensive carbonate-quartz veins, a phenomenon linked to the mobilization and mineralization of gold (Fu and Touret, 2014). The presence of CO_3^{2-}- and SO_4^{2-}-rich scapolite could potentially act as a buffer for pore fluids during such processes, influencing content of carbon and sulfur species of the liberated fluid due to the decomposition of scapolite. A similar scenario has been discussed by Morrissey and Tomkins (2020), where scapolite may significantly impact both fluid composition and its oxidation state.

Retrograde breakdown of SO_4^{2-}- and CO_3^{2-}-rich scapolite can occur relatively quickly during exhumation due to the combined effects of destabilization as scapolite minerals leave their lower crustal pressure–temperature stability field and the interaction with retrograde aqueous fluids. In contrast to a scenario described in Morrissey and Tomkins (2020), where scapolite breakdown under upper greenschist metamorphic conditions releases significant amounts of Cl, fluids released from scapolite from granulite-facies rocks would release fluids rich in oxidized S and C species with only a minor Cl component. Previous studies (e.g., Porter and Austrheim, 2017), however, have demonstrated that such retrograde fluids can contain substantial, externally-derived Cl. These fluids would be relatively oxidized, with elevated H_2SO_4/H_2S and may transport metals through the middle and upper crust as sulfide saturation is prevented, and primary igneous sulfides may be "remobilized" (see also Meng et al., 2021). Given the presence of chalcopyrite and pentlandite droplets within the granulites, fluids may become enriched in certain (base) metals due to the oxidation and breakdown (and subsequent mobilization) of these sulfides. Importantly, such S-rich fluids can be produced without direct input of magmas, but simply by the release of S and C from scapolite decomposition during exhumation and/or retrogression of granulite terranes. The transport of scapolite-bearing lower crust to mid and upper crustal levels can occur during extension related to orogenic collapse, or the uplift of core complexes (Fig. 8), or may occur in transpressive regimes, as in Madagascar (e.g., Martelat et al., 2000). It follows that, in addition to the S-release window ($\leq$550 °C) during prograde metamorphism (Tomkins, 2010) and the potential mobilization of metals, S may also be released at higher temperatures when granulites that contain S-rich scapolite undergo retrogression at middle to upper amphibolite-facies conditions. A schematic illustration of such processes is shown in Fig. 8 where mantle-derived intrusions, which also carry exsolved sulfides, infiltrate the surrounding host units in which sulfides, together with mantle-derived CO_2, react with the granulite-facies mineral assemblage to form scapolite. Magmatic scapolite can crystallize within cumulates and concentrate oxidized sulfur (and CO_2 as CO_3^{2-}), whereas the reduced sulfur forms interstitial sulfides and may also be trapped in major minerals as sulfide inclusions (Figs. 2, 8A, B). The co-existence of oxidized and reduced sulfur species suggests that fO_2 of the system was at, or very close to, the sulfide to sulfate transition (i.e., fence) (Jugo et al., 2005; Tomkins, 2010; Morrissey and Tomkins, 2020). As outlined above, lower crustal exhumation leads to destabilization of scapolite and the release of C and S as oxidized species and minor amounts of Cl, which, together with retrogressive aqueous fluids, leads to the breakdown of sulfides and the mobilization of base metals (Fig. 8C). Channeling of

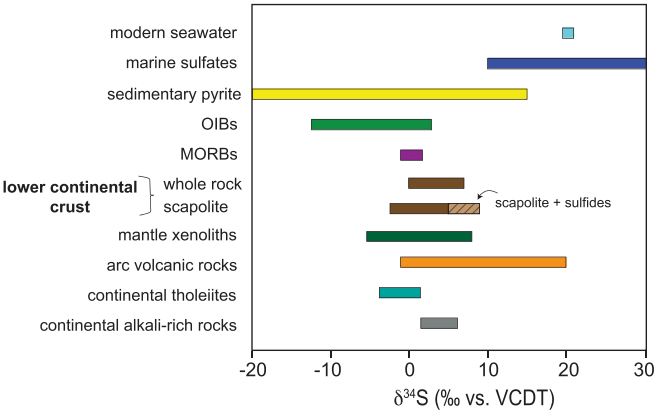

Fig. 7. Sulfur isotope signatures in different terrestrial reservoirs modified after Hammerli et al. (2017). S isotope ratios of marine sulfates/sedimentary pyrite are from Farquhar et al. (2010) and references therein. Sulfur isotope ratios of OIBs are taken from Sakai et al. (1984), Torssander (1989), Chaussidon et al. (1989), Cabral et al. (2013), and Dottin et al. (2020). The range of MORB S isotope ratios is from Kanehira et al. (1973), Sakai et al. (1984), and Labidi et al. (2012, 2013). Sulfur isotope ratios in the lower continental crust derived from whole rock analyses are from Hoefs et al. (1982), Iyver et al. (1992) and S isotope ratios in scapolite are from Hammerli et al. (2017) and this study. The highest δ^{34}S found in lower continental crust (hatched pattern) are from scapolite that coexist with sulfides that have lower δ^{34}S, and hence such S in scapolite is not representative of the whole rock. Sulfur isotope ratios in sulfides and whole rock from mantle rocks including xenoliths are from Chaussidon et al. (1989), Chaussidon and Lorand (1990), Ionov et al. (1992), Giuliani et al. (2016) and Wilson et al. (1996). Sulfur isotope data from arc volcanic rocks are from Ueda and Sakai (1984), Alt et al. (1993), Woodhead et al. (1987), de Hoog et al. (2001), and Marini et al. (2011). Continental tholeiites S isotope values are from Schneider (1970) and S isotope values from continental alkali-rich rocks are from Schneider (1970) and Harmon et al. (1987).

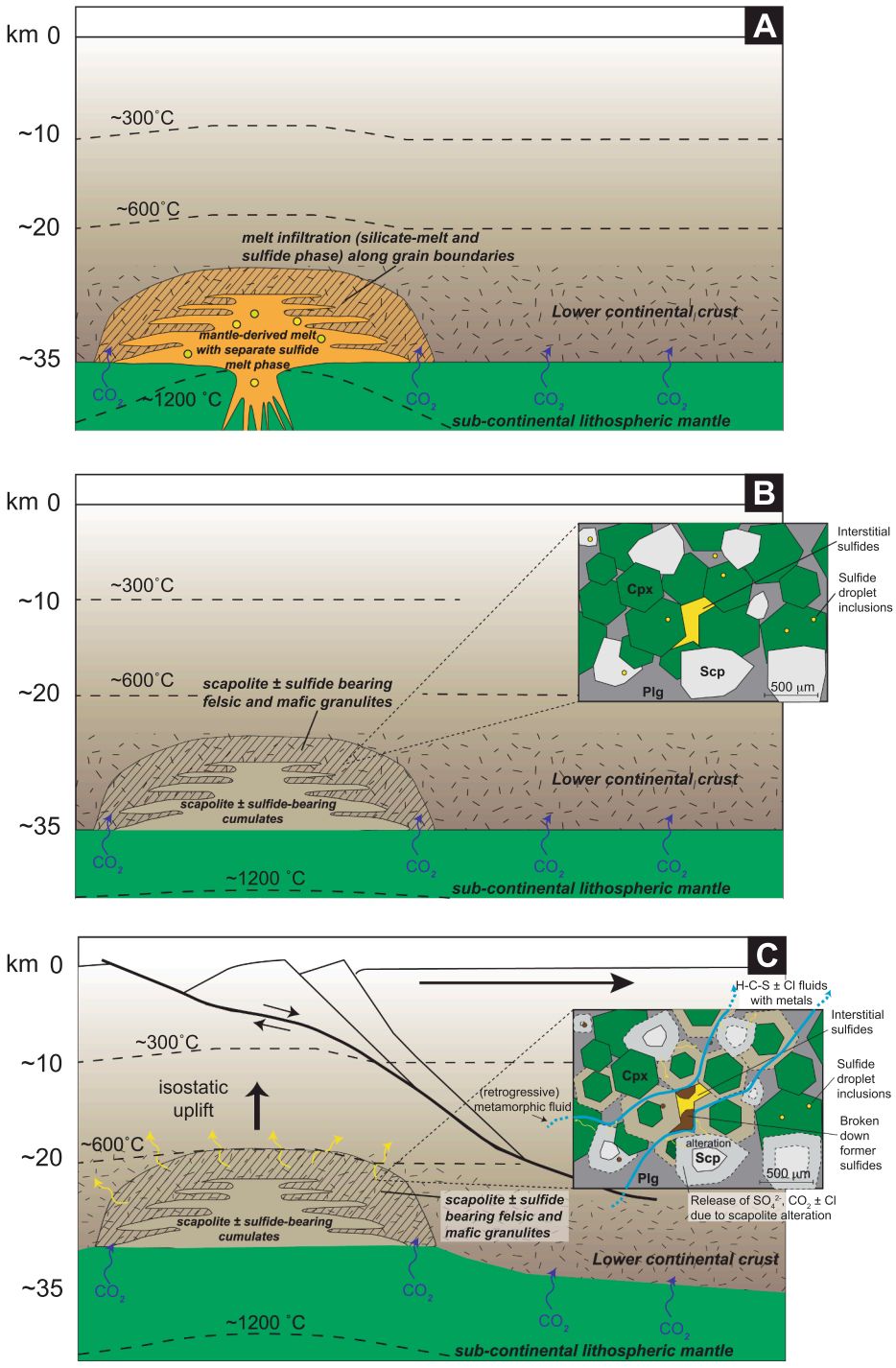

Fig. 8. A) Intrusion of mantle-derived melt into the lower crust. Sulfides are exsolved from the silicate melt and form separate phases. The silicate and sulfide melts infiltrate the surrounding (granulite facies) rocks through micro-conduits. B) As the mantle-derived intrusions cool and differentiate in the lower crust, they form crystal cumulates. These cumulates also host (former) interstitial sulfide melts, magmatic scapolite, and sulfide inclusions in major minerals (Figs. 1 and 2). C) Exhumation of the lower crust, such as in extensional regimes, transports scapolite-bearing granulites to mid-crustal levels where S-rich scapolite is no longer stable and begins to break down (i.e., during formation of a core complex). This process is accelerated by the infiltration of aqueous retrogressive fluids along grain-boundaries and pore-spaces. H_2O and the liberated CO_2, SO_4^{2-} ± Cl react and destabilize sulfides. The fluids become enriched in base metals (from sulfides) and infiltrate lithologies in the middle and upper crust, where they might become channelized and feed ore systems.

such fluids during deformation can lead to mineralization along major (fault or shear zone) structures.

While direct correlation between the exhumation of scapolite-bearing granulites and the mobilization and concentration of (base) metals has yet to be firmly established, examples of mineralization in retrogressed granulite-facies rocks have been documented in earlier studies, such as in regionally retrogressed granulites within the Limpopo Belt in southern Zimbabwe (e.g., Kolb et al., 2000). There, the sulfur isotope compositions of sulfides from mineralized zones yielded an average $\delta^{34}S$ of ~3.5 ‰, which coincidentally matches the average $\delta^{34}S$

of scapolites measured in our study and falls within the typical range of sulfur isotope ratios for the lower crust (Fig. 7). Other examples of fluids believed to originate from the deep crust (and metasomatized mantle) include the Danba gold deposit, located on the northwestern margin of the Yangtze Craton. This hypozonal mineralized system occurs in Paleozoic amphibolite-facies metasedimentary sequences at the edge of a core complex (Zhao et al., 2019). Mineralized systems in the Massif Central, France, where rapidly exhumed lower crustal blocks and regional faults extending into the deep crust created large-scale plumbing systems, are thought to be connected to the "granulitization" of the lower crust, from which mineralizing fluids were sourced (Bouchot et al., 2005). Goldfarb et al. (2007) noted a significant time gap between the formation of high-grade metamorphic rocks and their mineralization. This observation aligns with our model, as illustrated in Fig. 8, where time gaps between the formation of scapolite and the subsequent exhumation and release of metals are probable. However, it is noteworthy that sulfur-rich fluids enriched in metals can potentially migrate to shallower crustal depths before the onset of mineralization. Hence, fluids liberated from granulites do not necessarily generate mineralization in the high-grade rocks themselves. Drawing upon the current and previous studies, we deduce that fluids emanating from granulites would likely exhibit a sulfur isotope signature within the range of approximately $\delta^{34}S$ ~−2 to +10 ‰.

6.4. Estimate of total S and C stored in scapolite

The global S and C cycles are complex and there is ongoing debate about the amount and oxidation state of S released during slab subduction to the mantle wedge and eventually emitted by arc volcanoes, partially because of the large uncertainties in the S fluxes (Bekaert et al., 2021 and references therein). In addition to difficulties in estimating the S budget in subduction zones, some studies show that the ^{34}S-enriched signatures of some arc volcanic rocks are not due to "recycled" ^{34}S from slab-derived fluids (e.g., Li et al., 2020; Lee et al., 2018), but rather sourced from the deep arc crust. However, other studies (e.g., Bénard et al., 2018) suggest the opposite, and recently Rezeau et al. (2023) proposed that a mix of factors, including the formation of immiscible sulfide melts within primitive mafic magmas under lower crustal conditions, and subsequent gas release from ascending evolved melts can result in the elevated $\delta^{34}S$ values observed in both erupted arc lavas and volcanic gases. Like the sulfur cycle, the global CO_2 cycle is difficult to balance and net global ingassing estimates (i.e., transport of CO_2 into the deeper mantle) are much larger than global outgassing estimates (Bekaert et al., 2021 for a review). Calculated CO_2 outgassing, can, however change significantly if potential diffuse degassing is accounted for (Bekaert et al., 2021), or if metamorphic decarbonation reactions at forearc depths are considered (Stewart and Ague, 2020).

Scapolite group minerals can host significant quantities of sulfur and carbon in the lower crust. Scapolite is not ubiquitous in lower crustal rocks, and estimating the overall abundance in the deep crust is difficult due to several factors, including the alteration of lower crust rocks (i.e., destruction of scapolite). However, scapolite is frequently observed in unretrogressed granulite-facies rocks, and its significance in sulfur and carbon storage within various reservoirs can be estimated (Figs. 9 and 10). The surface reservoir, which consists of seawater, the oceanic crust and the continental crust, is estimated to contain significantly less S than the depleted mantle (7 % vs. 93 %, respectively, values from Chaussidon et al. 1989 and references therein) (Fig. 9A), and the continental crust hosts ~71 % of the total sulfur of the surface reservoirs (Fig. 9B). Assuming sulfur concentrations in the lower crust from Rudnick and Gao (2014), it is estimated that around 15 % of the continental crust's sulfur is concentrated in the lower crust (see Fig. 9C). The relative amount of the total S stored in scapolite within the lower crust depends on the abundance of scapolite-bearing rocks, the modal abundance of scapolite within these rocks, and the S content in scapolite itself. Fig. 9D illustrates how changes in the abundance of scapolite-bearing rocks and the modal proportion of scapolite within these rocks affect the percentage of sulfur stored in scapolite. This figure assumes a fixed sulfur content in scapolite of 1.5 wt%, which represents the average measured S content in scapolite in this study (see supplementary Figure S3 for additional scenarios with varying sulfur contents). As shown in Fig. 9D, the importance of scapolite as a S reservoir shifts significantly with changes in these abundance parameters. However, based on prior studies and admittedly limited datasets (e.g., Rudnick and Taylor, 1987; Moecher, 1988; Markwick and Downes, 2000; Yoshino and Satish-Kumar, 2001; Mansur et al., 2014), we estimate – using this as a working example – that up to 5 % of lower crustal rocks may contain SO_4^{2-}- and CO_3^{2-}-rich scapolite. Determining the average modal abundance of scapolite in these rocks is similarly difficult, as illustrated by our samples, which contain ~5 % to 30 % scapolite. Given this observed range and findings from previous studies, we estimate an average modal abundance of 5 % scapolite in scapolite-bearing lower crustal rocks. A simplified calculation, using the total area of continental crust estimated at 210.4×10^6 km^2 (Cogley, 1984), and an average thickness of the lower continental crust of 10.9 km (Hacker et al., 2015, derived from the seismic model CRUST 1.0), yields a lower crustal volume of $\sim 2.29 \times 10^9$ km^3. This calculation results in an estimated 5.7×10^6 km^3 of scapolite in the global lower continental crust, corresponding to an approximate scapolite content of 0.3 % by volume of the entire lower crust. Using an average density of sulfur- and carbon-rich scapolite of 2.75 g/cm^3 (Teertstra et al., 1999), we can calculate the sulfur budget. This example suggests that approximately 2.4×10^{20} grams of sulfur, or 10 % of the total sulfur in the lower crust, is hosted in scapolite, representing about 1.5 % of the total sulfur budget in the continental crust.

As for the above S calculations, it is assumed that the depleted mantle hosts more C than the surface reservoir, with the continental crust serving as the primary repository within the surface reservoir (Fig. 10A, B). Since, to our knowledge, no estimate of the C content in the lower crust exists to compare to the role of scapolite as a C host, we simply aimed to calculate the total amount of C stored in scapolite within the lower crust, based on varying scapolite abundances (Fig. 10C). For example, using the same parameters as for the S distribution calculations (i.e., 5 % of lower crustal rocks contain scapolite with a modal abundance of 5 % and an average C content in scapolite of 0.7 wt% from this study), we estimate the C stored in scapolite is approximately 1.1×10^{20} grams, representing less than 1 % of the surface reservoir's total C. In terms of the global S cycle, the above calculations permit an estimate of how much "new" scapolite-bearing lower crust has to be formed each year to balance the S cycle. Bekaert et al. (2021) estimated that ~87 % of the total S that enters subduction zones is accounted for by S outflux from arc volcanoes as well as S released from the mantle at, for example, mid oceanic ridges. To account for the remaining 13 %, approximately ~5 km^3 of new scapolite-bearing lower crust has to be formed each year (when using the above scenario of a 5 % modal abundance of scapolite in scapolite-bearing granulites, Fig. 9C). While these calculations involve many uncertainties, they show that scapolite in the lower crust may indeed play a role in the global S (and C) cycle as foreshadowed by Goldsmith (1976) and with potentially even greater impacts at regional

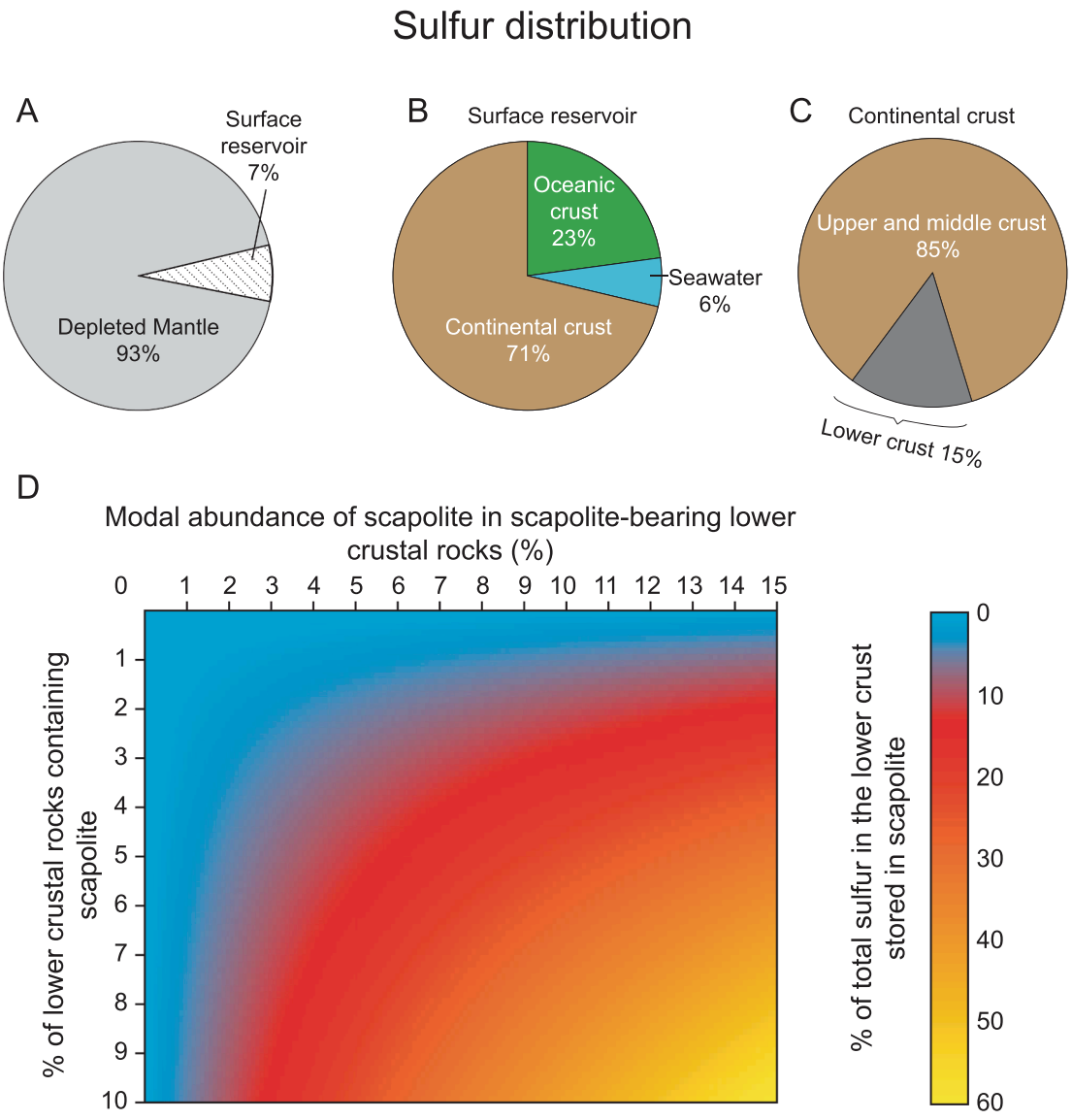

Fig. 9. Sulfur distribution in different terrestrial reservoirs. The surface reservoir consists of seawater, the oceanic crust and the continental crust. A) Shows that, compared to the depleted mantle, the surface reservoir contains much less sulfur. B) 71% of the surface reservoir's S is stored in the continental crust. C) The upper and middle crust contain approximately 85% of the continental crust's S, while the lower crust contains about 15%. D) Color-coded plot showing the distribution of S storage in the lower crust in relation to scapolite abundance. The X-axis represents the modal abundance of scapolite in scapolite-bearing lower crustal rocks (%), and the Y-axis indicates the proportion of lower crustal rocks containing scapolite (%). The color bar illustrates the percentage of the lower crust's total S stored in scapolite, with warmer colors representing higher proportions. The color bar is based under the assumption that the average S content of scapolite is 1.5 wt% as determined in this study. See text for details and calculations. Sulfur concentrations for the different reservoirs are from Chaussidon et al. (1989) and Rudnick and Gao (2014).

and local scales. Sulfur (and carbon) stored in scapolite will eventually be liberated during exhumation of these lower crustal rocks. However, these geodynamic mechanisms may function at different rates compared to other aspects of the sulfur (and carbon) cycle, such as the transfer of sulfur from the descending slab to the volcanic arc above it.

Future studies are essential to understand the distribution and behavior of sulfur and carbon in various tectonic settings, such as the lower crust of cratons and the lower continental crust above subduction zones, to determine whether oxidized forms of sulfur and carbon are more prominently stored in specific geodynamic and crustal

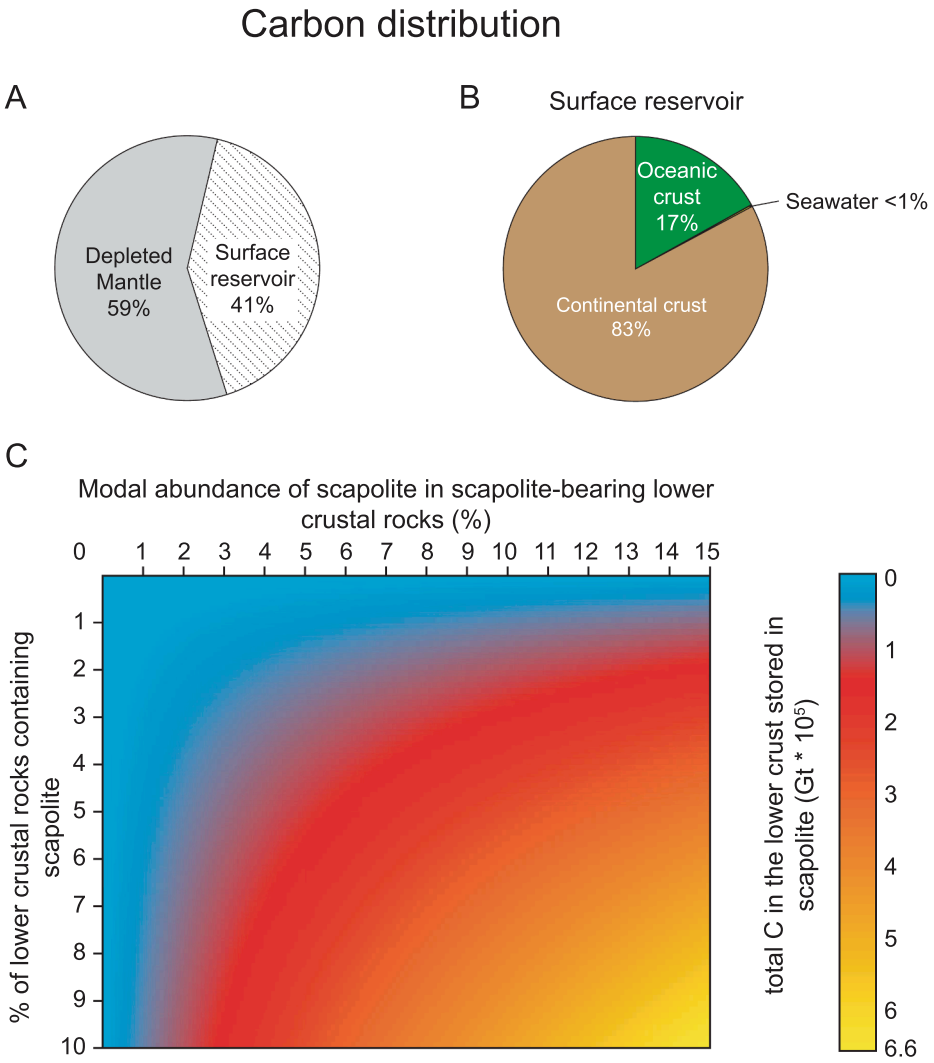

Fig. 10. Carbon distribution in different terrestrial reservoirs. A) Illustrates that the depleted mantle is thought to contain a greater amount of carbon than surface reservoir. B) The continental crust is the primary carbon reservoir within the surface reservoir. C) Color-coded plot depicting carbon storage distribution in the lower crust in relation to scapolite abundance. The X-axis shows the modal abundance of scapolite in scapolite-bearing lower crustal rocks (%), while the Y-axis represents the proportion of lower crustal rocks that contain scapolite (%). The color bar represents the calculated carbon storage (in gigatons $\times 10^5$) within scapolite in the lower crust. Warmer colors indicate higher total carbon contents stored in scapolite, assuming an average carbon content of 0.7 wt% in lower crustal scapolite, as determined in our study. Carbon contents for the different reservoirs are from Sleep and Zahnle (2001) and Aiuppa et al. (2021).

environments. This research could provide insights into the residence times of sulfur and carbon in the crust, as well as their potential for release during exhumation.

7. Conclusions

The major findings of this study are as follows:

- A relatively oxidizing environment with low aH_2O is likely crucial for scapolite formation. Together with scapolite, the presence of S-rich apatite supports elevated concentrations of oxidized sulfur in certain lower crustal regions.
- Scapolite in the lower crust can be either igneous or metamorphic in origin. The latter form via the reaction of magmatic sulfides and silicates, where the S and C may be transported to the lower crust from upper mantle zones or derived from supracrustal lithologies. In mafic granulites, the primary source of sulfur in scapolite is the mantle, deriving from (metasomatized) mantle reservoirs. This is consistent with prior research (Moecher et al., 1994), which suggested that CO_2 emanating from the mantle interacts with lower crustal lithologies to stabilize scapolite.
- We estimate that, globally, ~10 % of the lower crust's sulfur is hosted in scapolite. Certain lithologies are exceptionally rich in scapolite, with modal abundances of up to ~30 %, indicating that scapolite minerals locally concentrate substantial amounts of oxidized sulfur as well as CO_3^{2-}. Therefore, scapolite minerals play an important role in the sulfur (and carbon) flux between the mantle, the lower crust, and, upon scapolite destabilization, the middle and upper crust.
- The exhumation of scapolite-bearing lower crustal rocks can release and regulate fluids, influencing their redox conditions and potentially mobilizing base metals. The sulfur isotopic composition of fluids that derive sulfur from scapolite can vary, ranging from mantle values to heavier signatures, reaching +10 ‰ $\delta^{34}S$, indicative of the sulfur isotopic diversity in the (metasomatized) mantle and lower crust. Oxidized sulfur-rich fluids with sulfur isotope signatures akin to those found in the mantle can arise within the middle crust independently of mantle melt emplacement.

CRediT authorship contribution statement

Johannes Hammerli: Writing – original draft, Methodology, Investigation, Funding acquisition, Conceptualization. **Anthony I.S. Kemp:** Writing – review & editing, Resources, Conceptualization. **Anne-Sophie Bouvier:** Writing – review & editing, Resources, Methodology, Formal analysis. **Roberta L. Rudnick:** Writing – review & editing, Resources, Conceptualization. **Pierre Boivin:** Writing – review & editing, Resources. **Robert M. Holder:** Writing – review & editing, Resources. **Thomas Chacko:** Writing – review & editing, Resources. **Kevin Blake:** Writing – review & editing, Resources, Methodology.

Data availability

Data are available through Mendeley Data at https://doi.org/10.17632/b8ndnkj3sk.1.

Declaration of competing interest

The authors declare that they have no known competing financial interests or personal relationships that could have appeared to influence the work reported in this paper.

Acknowledgments

We would like to thank L. Zhang for the editorial handling of this paper and D. Harlov and two anonymous reviewers for their constructive feedback. Their insightful comments and suggestions have greatly improved the quality of this manuscript. Thi Hao Bui is thanked for conducting bulk scapolite S isotope analyses. Bradley Hacker is thanked for providing sample material. This work was funded by Swiss National Science Foundation grant PZ00P2_180095 to JH. RMH acknowledges support from the National Science Foundation, United States, under grant number NSF EAR 2022746.

Appendix A. Supplementary material

The supplementary material includes semi-quantitative EPMA maps showing sulfur content for a representative grain from each studied granulite sample. Additionally, the supplementary material contains a transmitted light image of a scapolite from sample 1636, showing the presence of oriented sulfide “needles”. We have also included additional figures to estimate the percentage of total sulfur stored in scapolite in the lower crust and the amount of carbon stored in scapolite, considering different sulfur and carbon contents in scapolite in addition to the average contents determined in this study. The supplementary material also contains the methodology for EPMA analyses conducted at the University of Alberta. Supplementary material to this article can be found online at https://doi.org/10.1016/j.gca.2025.01.010.

References

Aiuppa, A., Casetta, F., Coltorti, M., Stagno, V., Tamburello, G., 2021. Carbon concentration increases with depth of melting in Earth’s upper mantle. Nat. Geosci. 14, 697–703.

Alard, O., Lorand, J.-P., Reisberg, L., Bodinier, J.-L., Dautria, J.-M., O’Reilly, S., 2011. Volatile-rich metasomatism in montferrier xenoliths (Southern France): implications for the abundances of chalcophile and highly siderophile elements in the subcontinental mantle. J. Petrol. 52, 2009–2045.

Almeida, K.M.F., Jenkins, D.M., 2017. Stability field of the Cl-rich scapolite marialite. Am. Mineral. 102, 2484–2493.

Alt, J.C., Shanks, W.C., Jackson, M.C., 1993. Cycling of sulfur in subduction zones: The geochemistry of sulfur in the Mariana Island Arc and back-arc trough. Earth Planet. Sci. Lett. 119, 477–494.

Apen, F.E., Rudnick, R.L., Cottle, J.M., Kylander-Clark, A.R.C., Blondes, M.S., Piccoli, P. M., Seward, G., 2020. Four-dimensional thermal evolution of the East African Orogen: accessory phase petrochronology of crustal profiles through the Tanzanian Craton and Mozambique Belt, northeastern Tanzania. Contrib. Miner. Petrol. 175, 97.

Armstrong, J.T., 1991. Quantitative element analysis of individual microparticles with electron beam instruments. In: Heinrich, K.F.J., Newbury, D.E. (Eds.), Electron Probe Quantitation. Plenum Press, New York, pp. 261–315.

Aulbach, S., Krauss, C., Creaser, R.A., Stachel, T., Heaman, L.M., Matveev, S., Chacko, T., 2010. Granulite sulphides as tracers of lower crustal origin and evolution: An example from the Slave craton, Canada. Geochim. Cosmochim. Acta 74, 5368–5381.

Bebout, G.E., 1996. Volatile transfer and recycling at convergent margins: mass-balance and insights from high-P/T metamorphic rocks. AGU Geophys. Monogr. 96, 179–193.

Bekaert, D.V., Turner, S.J., Broadley, M.W., Barnes, J.D., Halldorsson, S.A., Labidi, J., Wade, J., Walowski, K.J., Barry, P.H., 2021. Subduction-driven volatile recycling: A global mass balance. Annu. Rev. Earth Planet. Sci. 49, 37–70.

Bénard, A., Klimm, K., Woodland, A.B., Arculus, R.J., Wilke, M., Botcharnikov, R.E., Shimizu, N., Nebel, O., Rivard, C., Ionov, D.A., 2018. Oxidising agents in sub-arc mantle melts link slab devolatilisation and arc magmas. Nat. Commun. 9, 3500.

Blattner, P., Black, P.M., 1980. Apatite and scapolite as petrogenetic indicators in granolites of Milford Sound, New Zealand. Contrib. Miner. Petrol. 74, 339–348.

Boivin, P., Camus, G., 1981. Igneous scapolite-bearing associations in the Chaine des Puys, Massif Central (France) and Atakor (Hoggar, Algeria). Contrib. Miner. Petrol. 77, 365–375.

Bouchot, V., Ledru, P., Lerouge, C., Lescuyer, J.-L., Milesi, J.-P., 2005. 5: Late Variscan mineralizing systems related to orogenic processes: The French Massif Central. Ore Geol. Rev. 27, 169–197.

Cabral, R.A., Jackson, M.G., Rose-Koga, E.F., Whitehouse, M.J., Antonelli, M.A., Farquhar, J., Day, J.M.D., Hauri, E.H., 2013. Anomalous sulphur isotopes in plume lavas reveal deep mantle storage of Archaean crust. Nature 496, 490–493.

Chaussidon, M., Albarede, F., Sheppard, S.M.F., 1989. Sulphur isotope variations in the mantle from ion microprobe analyses of micro-sulphide inclusions. Earth Planet. Sci. Lett. 92, 144–156.

Chaussidon, M., Lorand, J.-P., 1990. Sulphur isotope composition of orogenic spinel lherzolite massifs from Ariege (North-Eastern Pyrenees, France): An ion microprobe study. Geochim. Cosmochim. Acta 54, 2835–2846.

Chen, K., Tang, M., Lee, C.-T.-A., Wang, Z., Zou, Z., Hu, Z., Liu, Y., 2020. Sulfide-bearing cumulates in deep continental arcs: The missing copper reservoir. Earth Planet. Sci. Lett. 531, 115971.

Chesley, J.T., Rudnick, R.L., Lee, C.-T., 1999. Re-Os systematics of mantle xenoliths from the East African Rift: evidence for longevity of cratonic mantle and metasomatic Os addition. Geochim. Cosmochim. Acta 63, 1203–1217.

Cogley, J.G., 1984. Continental margins and the extent and number of the continents. Rev. Geophys. 22, 101–122.

Connolly, J.D., Cesare, B., 1993. C-O-H-S fluid composition and oxygen fugacity in graphitic metapelites. J. Metam. Geol. 11, 379–388.

Crowe, D.E., Vaughan, R.G., 1996. Characterization and use of isotopically homogeneous standards for in situ laser microprobe analysis of 34S/32S ratios. Am. Mineral. 81, 187–193.

Dawson, J.B., 1968. Recent researches on kimberlite and diamond geology. Econ. Geol. 63, 504–511.

de Hoog, J.C.M., Taylor, B.E., van Bergen, M.J., 2001. Sulfur isotope systematics of basaltic lavas from Indonesia: implications for the sulfur cycle in subduction zones. Earth Planet. Sci. Lett. 189, 237–252.

Dottin III, J.W., Labidi, J., Jackson, M.G., Woodhead, J., Farquhar, J., 2020. Isotopic evidence for multiple recycled sulfur reservoirs in the mangaia mantle plume. Geochem. Geophys. Geosyst. 21, e2020GC009081.

Du, Y., Qin, X., Barnes, C.G., Cao, Y., Dong, Q., Du, Y., 2014. Sulphide melt evolution in upper mantle to upper crust magmas, Tongling, China. Geosci. Front. 5, 237–248.

Farquhar, J., Wu, N., Canfield, D.E., Oduro, H., 2010. Connections between sulfur cycle evolution, sulfur isotopes, sediments, and base metal sulfide deposits. Econ. Geol. 105, 509–533.

Fu, B., Touret, J.L.R., 2014. From granulite fluids to quartz-carbonate megashear zones: The gold rush. Geosci. Front. 5, 747–758.

Giuliani, A., Fiorentini, M.L., Martin, L.A.J., Farquhar, J., Phillips, D.M., Griffin, W.L., LaFlamme, C., 2016. Sulfur isotope composition of metasomatised mantle xenoliths from the Bultfontein kimberlite (Kimberley, South Africa): Contribution from subducted sediments and the effect of sulfide alteration on S isotope systematics. Earth Planet. Sci. Lett. 445, 114–124.

Goldfarb, R.J., Hart, C., Davis, G., Groves, D., 2007. East Asian gold: deciphering the anomaly of phanerozoic gold in precambrian cratons. Econ. Geol. 102, 341–345.

Goldsmith, J.R., 1976. Scapolites, granulites, and volatiles in the lower crust Address as Retiring President of the Geological Society of America, Salt Lake City, Utah, October 1975. Geol. Soc. Am. Bull. 87, 161–168.

Goldsmith, J.R., Newton, R.C., 1977. Scapolite-plagioclase stability relations at high pressures and temperatures in the system $NaAlSi_3O_8$-$CaAl_2Si_2O_8$-$CaCO_3$-$CaSO_4$. Am. Mineral. 62, 1063–1081.

Hacker, B.R., Kelemen, P.B., Behn, M.D., 2015. Continental lower crust. Annu. Rev. Earth Planet. Sci. 43, 167–205.

Hamisi, J., Etschmann, B., Tomkins, A., Pitcairn, I., Pinter, Z., Wlodek, A., Morrissey, L., Micklethwaite, S., Trcera, N., Mill, S., Brugger, J., 2023. Complex sulfur speciation in scapolite – Implications for the role of scapolite as a redox and fluid chemistry buffer in crustal fluids. Gondw. Res. 121, 418–435.

Hammerli, J., Kemp, A.I.S., Barrett, N., Wing, B.A., Roberts, M., Arculus, R.J., Boivin, P., Nude, P.N., Rankenburg, K., 2017. Sulfur isotope signatures in the lower crust: A SIMS study on S-rich scapolite of granulites. Chem. Geol. 454, 54–66.

Hammerli, J., Greber, N.D., Martin, L., Bouvier, A.-S., Kemp, A.I.S., Fiorentini, M.L., Spangenberg, J.E., Ueno, Y., Schaltegger, U., 2021. Tracing sulfur sources in the crust via SIMS measurements of sulfur isotopes in apatite. Chem. Geol. 579, 120242.

Harlov, D.E., 2012. The potential role of fluids during regional granulite-facies dehydration in the lower crust. Geosci. Front. 3, 813–827.
Harlov, D.E., 2024. The potential role of sulfur during granulite-facies metamorphism, oxidation, and geochemical transformation of the granitoid lower crust. Petrology 32, 142–164.
Harlov, D.E., Hansen, E.C., 2005. Oxide and sulphide isograds along a Late Archean, deep-crustal profile in Tamil Nadu, south India. J. Metam. Geol. 23, 241–259.
Harmon, R.S., Hoefs, J., Wedepohl, K.H., 1987. Stable isotope (O, H, S) relationships in Tertiary basalts and their mantle xenoliths from the Northern Hessian Depression, W.-Germany. Contrib. Miner. Petrol. 95, 350–369.
Hilton, D.R., Fischer, T.P., Marty, B., 2002. Noble gases and volatile recycling at subduction zones. Rev. Miner. 47, 319–370.
Hoefs, J., Coolen, J.J.M., Touret, J., 1982. The sulfur and carbon isotope composition of scapolite-rich granulites from southern Tanzania. Contrib. Miner. Petrol. 78, 332–336.
Holder, R.M., Hacker, B.R., 2019. Fluid-driven resetting of titanite following ultrahigh-temperature metamorphism in southern Madagascar. Chem. Geol. 504, 38–52.
Holwell, D.A., Fiorentini, M.L., Knott, T.R., McDonald, I., Blanks, D.E., McCuaig, T.C., Gorczyk, W., 2022. Mobilisation of deep crustal sulfide melts as a first order control on upper lithospheric metallogeny. Nat. Commun. 13, 573.
Ionov, D.A., Hoefs, J., Wedepohl, K.H., Wiechert, U., 1992. Content and isotopic composition of sulphur in ultramafic xenoliths from central Asia. Earth Planet. Sci. Lett. 111, 269–286.
Iyver, S.S., de Oliveira, M.A.F., Hoefs, J., Krouse, H.R., 1992. Sulfur and carbon isotopes in scapolite-bearing granulites of the Sao Jose do Rio Pardo area. Brazil. J. South Am. Earth Sci. 6, 59–66.
Jugo, P.J., Luth, R.W., Richards, J.P., 2005. An Experimental Study of the Sulfur Content in Basaltic Melts Saturated with Immiscible Sulfide or Sulfate Liquids at 1300°C and 1·0 GPa. J. Petrol. 46, 783–798.
Ketcham, R.A., 2015. Technical Note: Calculation of stoichiometry from EMP data for apatite and other phases with mixing on monovalent anion sites. Am. Mineral. 100, 1620–1623.
Kita, N.T., Huberty, J.M., Kozdon, R., Beard, B.L., Valley, J.W., 2011. High-precision SIMS oxygen, sulfur and iron stable isotope analyses of geological materials: accuracy, surface topography and crystal orientation. Surf. Interface Anal. 43, 427–431.
Kolb, J., Kisters, A.F.M., Hoernes, S., Meyer, F.M., 2000. The origin of fluids and nature of fluid–rock interaction in mid-crustal auriferous mylonites of the Renco mine, southern Zimbabwe. Mineral Deposita 35, 109–125.
Korinevsky, V.G., Korinevsky, E.V., 2016. Unusual shape of pyrrhotite inclusions in scapolite of igneous rocks from the southernern Urals. Geol. Ore Deposits 58, 691–696.
Labidi, J., Cartigny, P., Birck, J.L., Assayag, N., Bourrand, J.J., 2012. Determination of multiple sulfur isotopes in glasses: A reappraisal of the MORB δ34S. Chem. Geol. 334, 189–198.
Labidi, J., Cartigny, P., Moreira, M., 2013. Non-chondritic sulphur isotope composition of the terrestrial mantle. Nature 501, 208–211.
Labidi, J., Cartigny, P., Hamelin, C., Moreira, M., Dosso, L., 2014. Sulfur isotope budget (32S, 33S, 34S and 36S) in Pacific–Antarctic ridge basalts: A record of mantle source heterogeneity and hydrothermal sulfide assimilation. Geochim. Cosmochim. Acta 133, 47–67.
LaFlamme, C., Martin, L., Jeon, H., Reddy, S.M., Selvaraja, V., Caruso, S., Hao, T., Roberts, M.P., Voute, F., Hagemann, S., Wacey, D., Littman, S., Wing, B., Fiorentini, M., Kilburn, M.R., 2016. In situ multiple isotope analysis by SIMS of pyrite, chalcopyrite, pyrrhotite, and pentlandite to refine magmatic ore genetic models. Chem. Geol. 444, 1–15.
Lee, C.-T.-A., Erdman, M., Yang, W., Ingram, L., Chin, E.J., DePaolo, D.J., 2018. Sulfur isotopic compositions of deep arc cumulates. Earth Planet. Sci. Lett. 500, 76–85.
Levien, L., Papike, J.J., 1976. Scapolite crystal chemistry: aluminum-silicon distributions, carbonate group disorder, and thermal expansion. Am. Mineral. 61, 864–877.
Li, J.-L., Schwarzenbach, E.M., John, T., Ague, J.J., Huang, F., Gao, J., Klemd, R., Whitehouse, M.J., Wang, X.-S., 2020. Uncovering and quantifying the subduction zone sulfur cycle from the slab perspective. Nat. Commun. 11, 514.
Lovering, J.F., White, A.J.R., 1964. The significance of primary scapolite in granulitic inclusions from deep-seated pipes. J. Petrol. 5, 195–218.
Manning, C.E., Aranovich, L.Y., 2014. Brines at high pressure and temperature: Thermodynamic, petrologic and geochemical effects. Precambr. Res. 253, 6–16.
Mansur, A.T., Manya, S., Timpa, S., Rudnick, R.L., 2014. Granulite-facies xenoliths in rift basalts of northern tanzania: age, composition and origin of archean lower crust. J Petrology 55, 1243–1286.
Marini, L., Moretti, R., Accornero, M., 2011. Sulfur isotopes in magmatic-hydrothermal systems, melts, and magmas. Rev. Mineral. Geochem. 73, 423–492.
Markwick, A.J.W., Downes, H., 2000. Lower crustal granulite xenoliths from the Arkhangelsk kimberlite pipes: petrological, geochemical and geophysical results. Lithos 51, 135–151.
Martelat, J.-E., Lardeaux, J.-M., Nicollet, C., Rakotondrazafy, R., 2000. Strain pattern and late Precambrian deformation history in southern Madagascar. Precambr. Res. 102, 1–20.
Mei, Y., Etschmann, B., Liu, W., Sherman, D.M., Barnes, S.J., Fiorentini, M.L., Seward, T. M., Testemale, D., Brugger, J., 2015. Palladium complexation in chloride- and bisulfide-rich fluids: Insights from ab initio molecular dynamics simulations and X-ray absorption spectroscopy. Geochim. Cosmochim. Acta 161, 128–145.
Meng, X., Kleinsasser, J.M., Richards, J.P., Tapster, S.R., Jugo, P.J., Simon, A.C., Kontak, D.J., Robb, L., Bybee, G.M., Marsh, J.H., Stern, R.A., 2021. Oxidized sulfur-rich arc magmas formed porphyry Cu deposits by 1.88 Ga. Nat. Commun. 12 (2189).
Miyoshi, T., Sakai, H., Chiba, H., 1984. Experimental study of sulfur between sulfate and sulfide isotope fractionation factors in high temperature melts. Geochem. J. 18, 75–84.
Moecher, D.P., 1988. Application of Scapolite Phase Equilibria and Carbon Isotope Systematics To High Grade Rocks: a Test of the CO_2-Flooding Hypothesis. Univ Michigan. PhD Thesis.
Moecher, D.P., 1993. Scapolite phase equilibria and carbon isotopes: constraints on the nature and distribution of CO_2 in the lower continental crust. Chem. Geol. 108, 163–174.
Moecher, D.P., Essene, E.J., Valley, J.W., 1992. Stable isotopic and petrological constraints on scapolitization of the Whitestone meta-anorthosite, Grenville Province, Ontario. J. Metam. Geol. 10, 745–762.
Moecher, D.P., Valley, J.W., Essene, E.J., 1994. Extraction and carbon isotope analysis of CO_2 from scapolite in deep crustal granulites and xenoliths. Geochim. Cosmochim. Acta 58, 959–967.
Morrissey, L.J., Tomkins, A.G., 2020. Evaporite-bearing orogenic belts produce ligand-rich and diverse metamorphic fluids. Geochim. Cosmochim. Acta 275, 163–187.
Newton, R.C., Goldsmith, J.R., 1975. Stability of the scapolite meionite ($3CaAl_2Si_2O_2 \cdot CaCO_3$) at high pressures and storage of CO2 in the deep crust. Contrib. Miner. Petrol. 49, 49–62.
Newton, R.C., Goldsmith, J.R., 1976. Stability of the end-member scapolites: $3NaAlSi_3O_8 \cdot NaCl$, $3CaAl_2Si_2O_8 \cdot CaCO_3$, $3CaAl_2Si_2O_8 \cdot CaSO_4$. Zeitschrift Für Kristallographie – Crystall. Mater. 143, 333–353.
Parra-Avila, L.A., Hammerli, J., Kemp, A.I.S., Rohrlach, B., Loucks, R., Lu, Y., Williams, I. S., Martin, L., Roberts, M.P., Fiorentini, M.L., 2022. The long-lived fertility signature of Cu–Au porphyry systems: insights from apatite and zircon at Tampakan. Philippines. Contrib Mineral Petrol 177, 18.
Porter, J.K., Austrheim, H., 2017. Sulphide formation from granulite-facies S-rich scapolite breakdown. Terra Nova 29, 29–35.
Qiu, Z., Fan, H.-R., Tomkins, A.G., Brugger, J., Etschmann, B., Liu, X., Xing, Y., Hu, Y., 2021. Insights into salty metamorphic fluid evolution from scapolite in the Trans-North China Orogen: Implication for ore genesis. Geochim. Cosmochim. Acta 293, 256–276.
Rakotondrazafy, M., Moine, B., Cuney, M., 1996. Mode of formation of hibonite ($CaAl_{12}O_{19}$) within the U-Th skarns from the granulites of S-E Madagascar. Contrib. Miner. Petrol. 123, 190–201.
Rezeau, H., Jagoutz, O., Beaudry, P., Izon, G., Kelemen, P., Ono, S., 2023. The role of immiscible sulfides for sulfur isotope fractionation in arc magmas: Insights from the Talkeetna island arc crustal section, south-central Alaska. Chem. Geol. 619, 121325.
Rielli, A., Tomkins, A.G., Nebel, O., Raveggi, M., Jeon, H., Martin, L., Avila, J.N., 2018. Sulfur isotope and PGE systematics of metasomatised mantle wedge. Earth Planet. Sci. Lett. 497, 181–192.
Rollinson, H.R., 1980. Mineral reactions in a granulite facies calc-silicate rock from Scourie. SJG 16, 153–164.
Rudnick, R.L., Fountain, D.M., 1995. Nature and composition of the continental crust: A lower crustal perspective. Rev. Geophys. 33, 267–309.
Rudnick, R.L., Gao, S., 2014. Composition of the continental crust. In: Holland, H.D., Turekian, K.K. (Eds.), Treatise on Geochemistry, second ed. Elsevier, Oxford, pp. 1–51.
Rudnick, R.L., Taylor, S.R., 1987. The composition and petrogenesis of the lower crust: A xenolith study. J. Geophys. Res. 92, 13981–14005.
Sakai, H., Marais, D.J.D., Ueda, A., Moore, J.G., 1984. Concentrations and isotope ratios of carbon, nitrogen and sulfur in ocean-floor basalts. Geochim. Cosmochim. Acta 48, 2433–2441.
Sammon, L.G., McDonough, W.F., Mooney, W.D., 2022. Compositional attributes of the deep continental crust inferred from geochemical and geophysical data. J. Geophys. Res. 127, e2022JB024041.
Schneider, A., 1970. The sulfur isotope composition of basaltic rocks. Contr Mineral and Petrol 25, 95–124.
Shaffer, M., Hacker, B.R., Ratschbacher, L., Kylander-Clark, A.R.C., 2017. Foundering triggered by the collision of India and Asia Captured in xenoliths. Tectonics 36, 1913–1933.
Shulaker, D.Z., Gordon, S.M., Hammerli, J., DesOrmeau, J.W., 2024. Fluid-Driven mass transfer during retrograde metamorphism and exhumation of the UHP Western Gneiss Region Terrane, Norway. Geochem. Geophys. Geosyst. 25 e2022GC010659.
Sleep, N.H., Zahnle, K., 2001. Carbon dioxide cycling and implications for climate on ancient Earth. J. Geophys. Res. Planets 106, 1373–1399.
Stewart, E.M., Ague, J.J., 2020. Pervasive subduction zone devolatilization recycles CO_2 into the forearc. Nat. Commun. 11, 6220.
Stolz, A.J., 1987. Fluid activity in the lower crust and upper mantle: mineralogical evidence bearing on the origin of amphibole and scapolite in ultramafic and mafic granulite xenoliths. Mineral. Mag. 51, 719–732.
Teertstra, D.K., Schindler, M., Sherriff, B.L., Hawthorne, F.C., 1999. Silvialite, a new sulfate-dominant member of the scapolite group with an Al-Si composition near the I4/m–P42/n phase transition. Mineral. Mag. 63, 321.
Teertstra, D.K., Sherriff, B.L., 1997. Substitutional mechanisms, compositional trends and the end-member formulae of scapolite. Chem. Geol. 136, 233–260.
Tomkins, A.G., 2010. Windows of metamorphic sulfur liberation in the crust: Implications for gold deposit genesis. Geochim. Cosmochim. Acta 74, 3246–3259.
Torró, L., Martin, R.F., Schumann, D., Cox, J., Gali, M.S., Melgareji Draper, J.C., 2018. The incipient flash melting of scapolite and plagioclase megacrysts in alkali basalts of the Olot suite, Catalunya, Spain, and at Chuquet Genestoux, Puy-de-Dôme, France. Eur. J. Mineral. 30 (1), 45–59.
Torssander, P., 1989. Sulfur isotope ratios of Icelandic rocks. Contrib. Miner. Petrol. 102, 18–23.

Touret, J., 1992. CO_2 transfer between the upper mantle and the atmosphere: temporary storage in the lower continental crust. Terra Nova 4, 87–98.
Ueda, A., Sakai, H., 1984. Sulfur isotope study of Quaternary volcanic rocks from the Japanese Islands Arc. Geochim. Cosmochim. Acta 48, 1837–1848.
von Knorring, O., Kennedy, W.Q., 1958. The mineral paragenesis and metamorphic status of garnet-hornblende-pyroxene-scapolite gneiss from Ghana (Gold Coast). Mineral. Mag. J. Mineral. Soc. 31, 846–859.
Vry, J., Powell, R., Golden, K.M., Petersen, K., 2010. The role of exhumation in metamorphic dehydration and fluid production. Nature Geosci 3, 31–35.
Wallace, P.J., 2005. Volatiles in subduction zone magmas: concentrations and fluxes based on melt inclusion and volcanic gas data. J. Volcanol. Geoth. Res. 140, 217–240.
Wang, Z., Yao, Z.-S., Jin, Z., Wang, Y., 2023. Experimental investigation on the transport of sulfide driven by melt-rock reaction in partially molten peridotite. J. Geophys. Res. Solid Earth, 128:e2022JB026065.
Whitney, D.L., Evans, B.W., 2010. Abbreviations for names of rock-forming minerals. Am. Mineral. 95, 185–187.
Wilson, A.F., 1976. Aluminium in coexisting pyroxenes as a sensitive indicator of changes in metamorphic grade within the Mafic Granulite Terrane of the Fraser Range, Western Australia. Contr Mineral and Petrol 56, 255–277.
Wilson, M.R., Kyser, T.K., Fagan, R., 1996. Sulfur isotope systematics and platinum group element behavior in REE-enriched metasomatic fluids: A study of mantle xenoliths from Dish Hill, California, USA. Geochim. Cosmochim. Acta 60, 1933–1942.
Wing, B.A., Farquhar, J., 2015. Sulfur isotope homogeneity of lunar mare basalts. Geochim. Cosmochim. Acta 170, 266–280.
Woodhead, J.D., Harmon, R.S., Fraser, D.G., 1987. O, S, Sr, and Pb isotope variations in volcanic rocks from the Northern Mariana Islands: implications for crustal recycling in intra-oceanic arcs. Earth Planet. Sci. Lett. 83, 39–52.
Yardley, B.W., 2005. 100th Anniversary Special Paper: metal concentrations in crustal fluids and their relationship to ore formation. Econ. Geol. 100, 613–632.
Yoshino, T., Satish-Kumar, M., 2001. Origin of scapolite in deep-seated metagabbros of the Kohistan Arc, NW Himalayas. Contrib. Miner. Petrol. 140, 511–531.
Zhao, H., Wang, Q., Groves, D.I., Deng, J., 2019. A rare Phanerozoic amphibolite-hosted gold deposit at Danba, Yangtze Craton, China: significance to fluid and metal sources for orogenic gold systems. Miner. Deposita 54, 133–152.